EGFL7 promotes immune evasion in glioma through its interaction with integrin β_2

Sukrit Mahajan[1], Philipp Abe[1,2], Fanny Ehret[1,3], Carina Fabian[1], Nora Heinig[1], Kathrin Barth[1], Marc Gentzel[4], Rajinder Gupta[5], Julieta Aprea[5], Paul Warnke[1], Beatrice Wasser[6], Stephan Grabbe[7], Marc Schmitz[8], Andreas Dahl[5], Frauke Zipp[6], Ulrike Schumann[1,*,†], Mirko HH Schmidt[1,*,†]

[1]Institute of Anatomy, Faculty of Medicine of TUD Dresden University of Technology, Dresden, Germany

[2]Institute for Clinical Genetics, University Hospital Carl Gustav Carus at TUD Dresden University of Technology and Faculty of Medicine of TUD Dresden University of Technology, Fetscherstrasse 74, 01307 Dresden, Germany

[3]German Center for Neurodegenerative Diseases (DZNE), Dresden 01307, Germany.

[4]Core Facility Molecular Analysis – Mass Spectrometry, Mass Spectrometry & Proteomics, Center for Molecular and Cellular Bioengineering (CMCB), TUD Dresden University of Technology, Dresden, Germany

[5]DRESDEN-concept Genome Center, Technology Platform at the Center for Molecular and Cellular Bioengineering (CMCB), TUD Dresden University of Technology, Dresden, Germany

[6]Department of Neurology, Focus Program Translational Neuroscience and Immunotherapy, Rhine Main Neuroscience Network, University Medical Center of the Johannes Gutenberg University Mainz, Mainz, Germany

[7]Department of Dermatology, University Medical Center of the Johannes Gutenberg University Mainz, Mainz, Germany

[8] Institute of Immunology, Faculty of Medicine Carl Gustav Carus, TUD Dresden University of Technology, Dresden, Germany

*Corresponding authors

† These authors contributed equally to this work.

Abstract:

Glioblastoma is the most aggressive form of malignant brain cancer, characterized by an immunosuppressive microenvironment and extensive angiogenesis. Epidermal growth factor-like protein 7 (EGFL7), a secreted pro-angiogenic factor that is highly expressed in the glioblastoma microenvironment (GME), has been implicated in immune evasion by other solid tumors, but its role in glioblastoma immune regulation remains unclear. Here, we studied the impact of EGFL7 in shaping the immune landscape in glioblastoma and identified underlying mechanisms. Single-cell transcriptomic profiling of immune cells from glioblastoma models revealed that EGFL7 promotes an immunosuppressive GME, characterized by increased infiltration of pro-tumorigenic macrophages and enhanced T cell exhaustion. Mechanistically, EGFL7 interacts with integrin β2 (ITGB2) on immune cells to mediate these effects. Genetic perturbation of the EGFL7-ITGB2 axis attenuated immunosuppression and significantly prolonged the survival of glioblastoma-bearing mice. In conclusion, our study provides unequivocal evidence that the EGFL7-ITGB2 axis acts as a critical

mediator of immunosuppression in glioblastoma and represents a potential therapeutic target for reprogramming the GME to prevent immune evasion in glioblastoma.

Introduction

Glioblastoma, the most aggressive primary brain tumor, is characterized by immune evasion, angiogenesis and resistance to currently available treatment strategies including surgical resection, radiotherapy and chemotherapy leading to tumor recurrence[1,2]. Consequently, the prognosis remains dismal, with a median survival of 18 months post diagnosis. Recent studies have highlighted the critical role of immune evasion in glioblastoma progression; however, the molecular mechanisms enabling tumor cells to evade immune surveillance remain poorly understood. The glioblastoma microenvironment (GME)[3,4], characterized by profound alterations to the healthy brain parenchyma, is a major driver of immune evasion. It constitutes a hostile milieu comprising anti-inflammatory myeloid populations that support tumor growth, along with exacerbated T cell exhaustion, which prevents an efficient anti-tumor immune response[5–7]. To curb the impact of the immunosuppressive GME and reprogram the anti-tumor immune response, several immunotherapies involving adoptive T cell therapy, immune checkpoint inhibitors (ICIs) and vaccines, have been tested[8–11]. Despite demonstrating clinical efficacy in non-small cell lung cancer (NSCLC)[12], melanoma[13] and various other solid tumors[14], their impact on glioblastoma remains largely limited and ineffective[15–18]. The failure of current immunotherapies in glioblastoma makes it imperative to identify tumor-intrinsic factors and underlying mechanisms that maintain an immunosuppressive GME for developing more effective therapies.

In this context, epidermal growth factor-like protein 7 (EGFL7), a secreted proangiogenic factor highly expressed in the GME[19], has been implicated in immune evasion in breast and lung cancer by inhibiting lymphocyte adhesion to the tumor vasculature[19,20]. Mechanistically, EGFL7 downregulates key endothelial adhesion molecules VCAM1 and ICAM1, thus facilitating immune escape[19]. Moreover, EGFL7 also contributes to glioma progression by promoting blood vessel formation and maturation within the tumor microenvironment[21].While it has been established as a modulator of tumor vasculature in glioblastoma, the influence of EGFL7 on immune regulation within the GME remains to be explored.

Therefore, in the current study, we used the murine glioma models to investigate how EGFL7 shapes the immune landscape in GME. We seek to identify distinct immune cell populations affected by EGFL7 expression by employing single cell RNA-sequencing (scRNA-seq) and precisely map these population within the GME, using spatial transcriptomics. Furthermore, proteomic profiling of the EGFL7 interactome, combined with mechanistic studies, will be leveraged to uncover potential pathways undertaken by EGFL7 to mediate immune modulation in glioblastoma. This will help to

develop novel therapeutic strategies targeting glioblastoma and advance our understanding of EGFL7 as a regulator of tumor progression.

Results

EGFL7 expression affects survival in glioblastoma

To investigate the clinical relevance of EGFL7 in glioblastoma, we analyzed patient samples from The Cancer Genome Atlas (TCGA). We observed that high EGFL7 expression in glioma patients was associated with shorter survival (Figure 1A).

We further evaluated the role of EGFL7 in glioma formation and survival of tumor-bearing mice through gain-of-function and loss-of-function studies (Extended Data Fig 1a). For the gain-of-function study, immunogenic murine GL261 glioma cells derived from C57BL/6 mice were retrovirally infected to ectopically express murine EGFL7 (mEGFL7) fused to a V5 tag and Strep-tag, followed by a P2A sequence and DsRed. Cells expressing DsRed alone served as a negative control**.** Cells were sorted using fluorescence-activated cell sorting (FACS) and the expression of DsRed and mEGFL7 in retrovirally transduced GL261 was determined using immunoblotting (Extended Data Fig. 1b). In the loss-of-function study, GL261-DsRed cells were intracranially implanted into the striatum of both EGFL7 knockout mice (EGFL7-/-) and their littermate controls (EGFL7+/+). We found that a constitutive EGFL7 knockout prolonged the survival of glioma-bearing mice with a median survival of 35 days compared to 28 days in the littermate controls (Figure 1B). We also found that EGFL7-/- mice had a comparatively smaller tumor 25 days post tumor implantation (TIMP), compared to the littermate controls (Figure 1B). In mEGFL7-glioma, ectopic EGFL7 expression was markedly elevated in the GME compared to control brain tissue as detected by immunostaining (Extended Data Fig. 1b). Subsequently, murine glioma cells ectopically expressing EGFL7 or DsRed were intracranially implanted into the striatum of wildtype C57BL/6J mice. Remarkably, mEGFL7 glioma-bearing mice demonstrated a significant reduction in survival, with a median lifespan of 30 days compared to 34 days in the control group (Figure 1C). Additionally, we observed a significant difference in tumor volume between mEGFL7 glioma-bearing mice and the DsRed control group at 28 days post TIMP (Figure 1D).

To corroborate our findings with GL261, SB28 murine glioblastoma cells were implanted (Extended Data Fig. 1c) in EGFL7 -/- mice, which exhibited longer survival compared to their littermate controls (Extended Data Fig. 1c), while a significant reduction in survival of mEGFL7-glioma bearing mice was observed (Extended Data Fig. 1d). These results suggest that EGFL7 expression has a deleterious effect on the survival of glioma-bearing mice. Further, we examined whether EGFL7 drives tumor progression by influencing the immune system. By employing our gain-of-function model in immunodeficient NSG mice, we observed no significant survival difference between mice implanted

with GL261-mEGFL7 or GL261-DsRed control cells (Figure 1E). Furthermore, while tumor size disparities were evident in immunocompetent mice 28 days post-implantation (Figure 1D), we observed no such difference in the tumor growth of immunodeficient mice (Figure 1F). Together, the data suggest that EGFL7 affects glioma progression by engaging the immune system.

Ectopic EGFL7 expression is associated with an increase of M2-like macrophages and T cell exhaustion in the tumor microenvironment

Having observed that EGFL7 is associated with reduced survival in immunocompetent - but not immunodeficient - glioma-bearing mice, we sought to determine the influence of EGFL7 on the immune response within the GME. Thus, we performed scRNA-seq on CD45+ immune cells sorted from the glioma tissue of the previously established gain-of-function and loss-of-function models employing GL261 cells, respectively (Figure 2A). To account for tumor heterogeneity, we included at least three biological replicates from each group, in both models. Uniform manifold approximation and projection (UMAP) dimension reduction was performed on 98,654 cells resulting in 31 clusters from 16 samples. Following quality control analysis, we predicted the different clusters based on the nomenclature provided by García-Vicente et al.[22] for clustering the CD45+ immune cells into myeloid and lymphoid populations (Figure 2B). The myeloid cluster comprised mainly macrophages, microglia and dendritic cells, while the lymphoid cluster was composed of T cells, NK cells and a small amount of B cells that were not further analyzed.

Using the immune cell atlas[23], macrophages were identified as the largest cluster in the myeloid population. Following supervised clustering, we specifically analyzed the macrophage and microglia cluster to determine the impact of EGFL7 (Figure 2C). Interestingly, mEGFL7-glioma tissue demonstrated a substantial accumulation of anti-inflammatory M2-like macrophages (Figure 2C-D), marked by a higher percentage of hypoxia-associated macrophages expressing *Arg1*$^{+}$ *Bnip3*$^{+}$ *Adam8*$^{+}$, myeloid-derived suppressor cells (MDSCs) expressing S100a9^{+}, and secreted phosphoprotein 1 (Spp1)-expressing macrophages (*Spp1+ Mrc1+*) as compared to DsRed control (Extended Data Fig. 2a). We also observed an increase in the microglial population (*Tmem119*$^{+}$ *P2ry12*$^{+}$) compared to DsRed control. Concurrently, a drastic reduction in pro-inflammatory M1-like macrophages (*Cd80*$^{+}$ *Cd86*$^{+}$) was observed from the macrophage cluster of mEGFL7-glioma tissues, suggesting a reduction in anti-tumor immunity (Figure 2D).

In contrast to the gain-of-function study, scRNA-seq analysis from EGFL7-/- mice revealed a decrease in immunosuppressive lipid-associated macrophages (*Fabp5+ Gpnmb+ Lgals3+*), which have been shown to promote tumor proliferation in glioblastoma[24,25]. In addition, we observed a substantial increase in transitory macrophages (*Ciita+ Adamdec1+*), immune cells in the process of differentiating from monocytes into macrophages (Extended Data Fig. 2b).

Further, the influence of EGFL7 on the lymphoid cluster with a specific focus on the largest population, i.e., T cells, was investigated (Figure 2B). The T cell cluster was resolved into different subtypes using clustering based on the T cell atlas[26] along with the identification of differentially expressed genes (Figure 2E, Extended Data Fig. 2c). Further analysis of these clusters revealed a higher percentage of exhausted T cells (*Pdcd1*$^{+}$ *Lag3*$^{+}$ *Gzma*$^{-}$) and regulatory T cells (*Foxp3*$^{+}$ *Il2ra*$^{+}$) (Figure 2F, Extended Data Fig. 2d) in mEGFL7 glioma mass compared to DsRed control. In addition, the CD4+ T helper 1 (Th1) cells were drastically reduced in the presence of ectopic EGFL7 expression, while no change was observed in the proportion of double negative (DN), CD4+ T helper 2 cells and proliferating T cells (Figure 2F). In contrast, scRNA-seq analysis of T cells from the EGFL7 knockout mice revealed a drastic increase in the terminal effector CD8+ T cell population (*Gzma*$^{+}$ *Gzmb*$^{+}$ *Gzmk*$^{+}$) as compared to littermate controls (Extended Data Fig. 2e-f). Meanwhile, the regulatory T cells (Tregs) exhibited an increase in the glioma tissues in the knockout mice.

Immune cell populations altered in our single cell analyses were validated by flow cytometry. A significant increase in M2-like macrophages (CD206^{+} ARG1^{+}), MDSCs (CD11B^{+} GR1^{+}) and microglia (CD45^{+low} CD11B^{+high}) with a declining trend for M1-like pro-inflammatory macrophages (CD80^{+} INOS2^{+}) was observed in mEGFL7-expressing tumor tissues (Figure 2G). Flow cytometry analysis of the myeloid populations in the glioma-bearing EGFL7-/- mice revealed a significant increase in the macrophage population (F4/80+ CD11b+) with a concurrent decrease in the MDSCs (Gr1+ CD11b+) in the glioma mass as compared to littermate controls (Extended Data Fig. 3a). However, no difference was observed in the microglial population.

Flow cytometry analysis of different T cell populations revealed an increased percentage of exhausted T cells in mEGFL7-glioma tissue with a concurrent rise in the regulatory T cell population (Figure 2H), which corroborated our transcriptomic analysis of T cells. In addition, proteomic analysis of T cells in the loss-of-function study revealed a significant increase in the overall CD8+ T cells along with the effector T cell population in the glioma mass of EGFL7-/- mice compared to their littermate controls (Extended Data Fig. 3b). However, a decrease in Tregs was observed with flow cytometry, which was in contrast to the increased percentage seen in the transcriptomic data (Extended Data Fig. 3b).

Overall, the high percentage of exhausted T cells in the presence of EGFL7 led us to assess whether EGFL7 directly influences T cell exhaustion. To examine this, we isolated T cells from the spleens of healthy wild-type mice and cultured them under *in vitro* conditions (Figure 2I). T cell activation was induced using plate-bound anti-CD3 and anti-CD28 antibodies. In parallel, purified recombinant murine EGFL7 protein was added to the culture medium to evaluate the effect of EGFL7. After five days, the percentage of effector CD8+ T cells was assessed to determine the impact of EGFL7 on T cell activation. In the presence of EGFL7, we observed a significant reduction in the effector CD8+ T

cell population ($GzmB^+$ $Ifn\gamma^+$) compared to controls (Figure 2I). This finding aligns with our *in vivo* transcriptomic analysis, showing that EGFL7 promotes T cell exhaustion, and its knockout is associated with an increase in effector CD8+ T cells (Figure 2E-F and Extended Data Fig. 2e-f).

EGFL7 expression affects immune cell distribution in GME

While our single cell analysis revealed EGFL7 as a mediator of immunosuppression, associated with an increased percentage of pro-tumorigenic M2-like macrophages and extensive T cell exhaustion, investigating the spatial organization of these immune cell populations within the GME became pertinent for delineating the function of EGFL7. Accordingly, we employed the EGFL7-/- mice and their littermate controls to determine whether EGFL7 influences the spatial distribution of immune cells, which is critical for understanding its role in immune modulation and tumor immune evasion. Accordingly, 25 days post TIMP, cryo-sections of the brain from GL261 tumor-bearing mice were subjected to spatial transcriptomics using 10x Visium.

The spatial clusters in the brain sections were identified and the tumor tissue was further classified into tumor core (including tumor core and tumor shell_1) and tumor shell (comprising of tumor shell_2) (Figure 3A) to delineate the distribution of different immune cell populations in glioma in the context of EGFL7 expression. Given the heterogeneity of the glioma tissue, attributed to different cell types and their spatial organization within the GME, we set out to identify the cellular architecture in our mouse model. Different cell types including immune cells, GL261 glioma cells, astrocytes and endothelial cells, among others, were predicted based on the study by García-Vicente et al.[22] (Figure 3B). Prediction scores revealed a clear distinction between the tumor and immune cell population. Annotations from the single cell analysis of the loss-of-function were used to predict the different clusters within the immune cell population. We focused specifically on the immune cell clusters and observed that macrophages and T cells exhibited distinct spatial heterogeneity across the tumor core, tumor shell, and neighboring healthy brain tissue (Figure 3C-D). In particular, knockout of EGFL7 mildly affected the distribution of macrophages as M1-like macrophages and lipid-associated macrophages were relatively increased in the glioma mass of EGFL7-/- mice compared to littermate controls. While lipid-associated macrophages were prevalent in the tumor core of both EGFL7+/+ and EGFL7-/- mice, hypoxia associated macrophages predominantly occupied the tumor shell (Figure 3D).

However, the distribution of T cells was strongly affected by knocking out EGFL7. In particular, CD4+ naïve T cells showed a small increase in tumor core of EGFL7-/- mice compared to littermate controls, with EGFL7 largely restricting them in the tumor shell (Figure 3D). Interestingly, a high percentage of terminal effector CD8+ T cells were observed in the tumor core of EGFL7-/- mice compared to their littermate control (Figure 3D). In contrast, Tregs were abundant throughout the brain tissue along with the tumor tissue in both EGFL7-/- and littermate controls. The impact of

EGFL7 on the spatial distribution of CD4+ and CD8+ cells suggested it has a strong influence on the infiltration pattern of T cell population, which we validated using histological analysis.

Histological analyses of paraffin embedded brain sections revealed that knockout of EGFL7 causes an increased percentage of CD8+ and CD4+ T cells in the tumor core compared to the glioma mass of littermate controls (Figure 3E). In contrast, the Tregs showed a significant decrease when EGFL7 was knocked out while endogenous EGFL7 expression led to a high infiltration of these cells within the tumor core (Figure 3E). Taken together, our data show that EGFL7 is associated with a marked decrease in CD8+ T cells and CD4+ T cells within the glioma mass, suggesting that EGFL7 not only impedes effector T cell function (Figure 2I) but also its infiltration (Figure 3D-E). Thus, findings from spatial transcriptomics analysis underscore the role of EGFL7 in mediating the inhibition of effector and helper T cell recruitment and sequestering pro-inflammatory M1-like macrophages away from the tumor core, thereby facilitating tumor progression and immune evasion.

EGFL7 interactome identifies immune cell specific ITGB2 as a novel interaction partner

Our *in vivo* analysis revealed that EGFL7 alters immune cell populations, prompting us to investigate the underlying molecular mechanism. EGFL7 has been implicated in suppressing T cell recruitment in breast and lung carcinoma by downregulating adhesion molecules[19]. In addition, spatial transcriptomics and histological analysis revealed reduced CD8+ T cell infiltration in EGFL7-expressing gliomas (Figure 3E-F). However, while previous studies focused on endothelial cell receptors as targets, we explored whether EGFL7 directly modulates immune cells through interactions with key immune regulatory proteins. Therefore, we analyzed the EGFL7 interactome in glioma tissue using co-immunoprecipitation in our gain-of-function model.

Following tumor growth, mEGFL7-tumor tissue was lysed, and V5-tagged EGFL7 was pulled down using an anti-V5 antibody. By utilizing DsRed-tumors as a negative control, we accounted for any non-specific binding that might occur. Next, the immunoprecipitated samples were analyzed using liquid chromatography-based mass spectrometry (Figure 4A). Gene ontology analysis of the EGFL7 interactome using Gorilla[27] and Cytoscape[28] identified the most significant biological processes which involved proteins from the interactome. We narrowed our focus to those affecting immune cell response in glioma – specifically, the regulation of cell adhesion and the positive regulation of immune response (Figure 4B). Among the proteins identified in the co-immunoprecipitation assay – and implicated in both biological processes integrin β_2 (ITGB2), an immune cell specific receptor, was highly abundant (Figure 4C) followed by integrin β_1 (ITGB1). Therefore, we focused on ITGB2, motivated by emerging evidence of its involvement in modulating immune cell functions in different tumor entities[29].

We confirmed the protein interactions identified in our mass spectrometry-based EGFL7 interactome analysis *in vitro* by transfecting HEK293-EBNA cells with plasmid constructs expressing different

genes of interest. Cells were co-transfected with plasmid constructs expressing either EGFL7 or DsRed (negative control) tagged to Flag-tag (Figure 4D; left), alongside separate expression vectors encoding ITGB2, ITGB3 (used as positive control) and ITGB5 gene, respectively tagged to V5. Using an anti-V5 antibody for the immunoprecipitation assay, we observed that EGFL7 was co-immunoprecipitated with ITGB2, ITGB3 and ITGB5, whereas the negative control DsRed was not pulled down with any integrins (Figure 4D; right). Since integrins function as heterodimeric complexes comprising of α- and β-subunits rather than isolated monomers, we further investigated the interaction of EGFL7 with the α-integrin partners of ITGB2, namely integrin-α_D (ITGAD or Cd11d), integrin-α_L (ITGAL or Cd11a), integrin-α_M (ITGAM or Cd11b) and integrin-α_X (ITGAX or Cd11c) which were all Myc-tagged. We used ITGAV and ITGB3 as positive controls as previously described[30]. Using an anti-Flag antibody, EGFL7 was selectively pulled down alongside ITGB3 and ITGB2 and their respective α-integrin partners, as shown in Figure 4E. In contrast, the negative control DsRed did not co-immunoprecipitate any integrin proteins. Among the α-integrin partners, integrin α_L (ITGAL) showed the strongest interaction, marking it as the most abundant interactor with ITGB2-bound EGFL7 (Figure 4E).

EGFL7-ITGB2 interaction prevents immune cell migration and promotes T cell exhaustion

The interaction of EGFL7 with ITGB2 suggested that EGFL7 might be directly influencing the immune system in the GME as already observed in our scRNA-seq and spatial transcriptomics analyses. It is well known that ITGB2 pairs with ITGAL to form the LFA-1 complex, which is involved in T cell migration and differentiation[31]. Similarly, ITGB2 associates with ITGAM to form the MAC-1 complex, a key mediator of myeloid cell chemotaxis and adhesion[32,33]. Based on these established roles, we investigated the migration capacity of immune cells *in vitro* (Figure 5A; Extended Data Fig. 4a) in the presence of purified EGFL7 protein with C-C motif chemokine ligand (CCL2) serving as a chemoattractant.

To assess its role in immune cell migration, EGFL7 was added with mouse splenocytes to the transwells (Extended Data Fig 4b). The immune cells which migrated to the lower chamber were quantified. CCL2 mediated chemoattraction significantly increased immune cell migration compared to the control medium (Figure 5A and Extended Data Fig. 4c). Interestingly, EGFL7 inhibited immune cell migration when co-incubated with immune cells in the top chamber, as evidenced by a reduction in migrating cells compared to the control medium (Figure 5A and Extended Data Fig. 4c). Even in the presence of CCL2 in the lower chamber, EGFL7 inhibited immune cell migration when incubated with immune cells, demonstrating its anti-migratory effect on these cells. This suggested that EGFL7 through its interaction with receptors on immune cells may influence the migration of immune cell populations *in vitro* and could possibly prevent the escape of T cells from the glioblastoma tissue or their infiltration into the tumor microenvironment.

EGFL7 broadly affects immune cell migration through its interaction with ITGB2

Building on the observed impact of EGFL7 on immune cell migration in the presence of CCL2, we investigated whether ITGB2 blockade modulates this process. Since ITGB2 is known to mediate T cell recruitment[34], we used a neutralizing antibody against ITGB2 (abITGB2) in combination with purified EGFL7 to evaluate its effect on immune cell migration under CCL2 stimulation. Thus, CD45+ immune cells isolated from mouse spleen were incubated with abITGB2, purified EGFL7, or a combination of both. In the presence of CCL2, both treatments similarly reduced immune cell migration compared to the CCL2 control (Figure 5B and Extended Data Fig. 4d). More importantly, the combination of abITGB2 and purified EGFL7 resulted in further reduction of immune cell migration (Figure 5B and Extended Data Fig. 4d). To delineate cell type-specific effects of EGFL7, we isolated T cells from the spleen and Cd11b+ myeloid cells from the bone marrow and subjected them to the same experimental conditions as in Figure 5B. In the presence of CCL2, we observed only a slight reduction in myeloid cell migration by either EGFL7 or abITGB2 alone, however their combination significantly decreased their migration (Figure 5C). In contrast, both EGFL7 and abITGB2 strongly inhibited T cell migration even in the presence of CCL2 (Figure 5D). Moreover, their combination further decreased the migration capacity of T cells compared to either treatment alone. These findings suggest that the EGFL7-ITGB2 axis plays a synergistic role in immune cell trafficking, especially in the case of T cell migration. Taken together, the data shows EGFL7 inhibits immune cell migration, partly through its interaction with ITGB2.

EGFL7-ITGB2 axis mediates immunosuppression in glioblastoma

On encountering that EGFL7 might be working in conjunction with ITGB2 to modulate the immune cells in the GME, we utilized an *in vivo* mouse model with inducible ITGB2 expression. GL261 cells expressing either DsRed (control) or mEGFL7 were stereotactically implanted into the striatum of mice lacking ITGB2 in hematopoietic stem cells (HSCs) ($ITGB2^{\Delta HSC}$ mice) and their littermates ($ITGB2^{fl/fl}$; controls). Due to the capacity of HSCs to give rise to various immune cell lineages, $ITGB2^{\Delta HSC}$ mice lacked ITGB2 expression in all hematopoietic cell-derived immune cell populations. Survival analysis demonstrated that $ITGB2^{\Delta HSC}$ mice bearing DsRed-gliomas had a prolonged life span compared to their $ITGB2^{fl/fl}$ littermates (Figure 5E). Moreover, $ITGB2^{\Delta HSC}$ mice had comparatively smaller tumors at 28 days post TIMP compared to littermate controls (Figure 5F). Additionally, a significant survival advantage was also observed in mEGFL7 glioma-bearing mice when ITGB2 was knocked out compared to littermate controls (Figure 5G). We also observed a significantly smaller tumor volume in GL261-mEGFL7 implanted $ITGB2^{\Delta HSC}$ mice compared to their littermates (Figure 5H). These findings suggest that EGFL7, in conjunction with ITGB2, contributes to glioma progression, and that disrupting this interaction enhances survival - even in the context of

mEGFL7 tumor-bearing mice. Next, we set out to determine the underlying cause of this enhanced survival.

In ITGB2$^{fl/fl}$ control mice, mEGFL7-expressing gliomas displayed a significantly higher proportion of exhausted T cells (55% of CD8+ T cells) compared to DsRed-expressing tumors (20% of CD8+ T cells). Conversely, ITGB2 deletion in ITGB2$^{\Delta HSC}$ animals markedly reduced T cell exhaustion to 33% in mEGFL7-expressing gliomas, with no significant differences observed between DsRed-gliomas from ITGB2$^{\Delta HSC}$ (19%) and ITGB2$^{fl/fl}$ mice (20%) (Figure 5I). Interestingly, mEGFL7-expressing gliomas displayed a significantly higher proportion of hypoxia associated macrophages (80% of Arginase +/CD206+ cells) compared to DsRed-expressing tumors (40% of Arginase +/CD206+ cells) in ITGB2$^{fl/fl}$ mice (Figure 5J). Moreover, a significant reduction of these pro-tumorigenic macrophages was observed upon deletion of ITGB2 in ITGB2$^{\Delta HSC}$ animals in mEGFL7-expressing gliomas, with no significant differences observed between DsRed-gliomas (Figure 5J). Taken together, these findings suggest that mEGFL7 plays a major role in promoting T cell exhaustion and causing increased infiltration of pro-tumorigenic macrophages in glioma. Disrupting the EGFL7-ITGB2 interaction rescues this effect.

EGFL7 blockade in conjunction with anti-PD1 therapy improves survival of glioma bearing mice

We observed that EGFL7 promotes T cell exhaustion, a key mechanism underlying the impaired anti-tumor immune response in glioma. This finding suggested that targeting EGFL7 may mitigate T cell exhaustion and improve the anti-tumor immunity. Thus, EGFL7 was targeted and in parallel, anti-PD1 therapy was evaluated in our model, as PD1 is a well-established immune checkpoint which inhibits cytotoxic T cells from targeting tumor cells.

GL261-DsRed and GL261-mEGFL7-DsRed cells were implanted into the mouse striatum and tumor progression was monitored via MRI. Two weeks after tumor engraftment, mice were intraperitoneally injected on days 16, 21, and 26 with antibodies targeting murine EGFL7 (abEGFL7) or PD1 (abPD1), a combination of both, or an isotype (IgG) control (Figure 6A). Kaplan-Meier survival analysis revealed that the combinatorial therapy with anti-PD1 and anti-EGFL7 led to an increase of 17-22% increase in median survival - extending the lifespan of DsRed glioma-bearing mice from 33 to 40 days (Figure 6B) and of mEGFL7-glioma bearing mice from 28 to 36 days (Figure 6C), respectively – relative to the the IgG control. In addition, anti-PD1 and anti-EGFL7 monotherapies did not have an effect on the survival of glioma-bearing mice implanted with GL261-DsRed or GL261-mEGFL7, compared to IgG control.

In summary, our data show that dual targeting of EGFL7 and PD1 improves the survival of glioma-bearing mice in the gain-of-function model. These promising results support clinical evaluation of combined EGFL7 and PD1 inhibition as a potential therapeutic strategy for glioma patients.

Discussion:

Glioblastoma is the most aggressive form of brain tumor, and despite ongoing therapeutic advancements, it remains incurable. The median overall survival for glioblastoma patients undergoing treatment is 15-18 months post diagnosis, underscoring the pressing need for novel therapeutic approaches. Extensive research has revealed several hallmarks of glioblastoma, with immune evasion playing a prominent role in tumor progression. Given the pronounced local immunosuppression within the GME, immunotherapy has emerged as an alternative approach to the currently available therapies for glioblastoma treatment. However, recent clinical trials - including CheckMate143 (NCT02017717) evaluating anti-PD1 therapy combined with bevacizumab[35], CheckMate 498 (NCT02617589) assessing nivolumab with radiotherapy, and CheckMate 548 (NCT02667587) evaluating chemoradiotherapy paired with anti-PD1 immunotherapy[16] - have failed to achieve the desired improvements in overall survival. These studies indicate that anti-PD1 monotherapy and combinatorial therapy involving radiotherapy or chemotherapy - fails to elicit an effective immune response against glioma. Therefore, identifying and targeting immune modulatory factors driving immune escape mechanisms may prove beneficial to reinvigorate the anti-tumor immune response in glioblastoma and help develop more effective treatment regimens.

In this context, we investigated the role of the pro-angiogenic protein EGFL as an immunomodulatory factor in GME. Previous studies in breast and lung cancer have demonstrated that EGFL7 downregulates endothelial adhesion molecules, including VCAM1 and ICAM1, thereby impairing lymphocyte adhesion and their subsequent infiltration into tumor tissue[19,20]. However, the specific impact of EGFL7 on immune regulation within the glioma microenvironment remains insufficiently understood. In the current study, we discovered a novel immunoregulatory role of the pro-angiogenic factor EGFL7 within the GME. Our results demonstrate that EGFL7 promotes glioma progression by driving immune cell dysfunction. Its expression correlates with enhanced infiltration of pro-tumorigenic M2-like macrophages and decreased anti-tumorigenic M1-like macrophages - a phenotype reversed in EGFL7-/- mice. Interestingly, human gliomas are known to polarize macrophages towards an anti-inflammatory state that promotes tumor growth by suppressing the local immune response[36,37]. The impact of EGFL7 on macrophages is particularly highlighted as these cells constitute the majority of the immune infiltrate within the GME.

Additionally, we identified that EGFL7 expression impacts T cell exhaustion and increases infiltration of regulatory T cells, leading to an immunosuppressing environment. It was observed that EGFL7 had a stronger effect on the spatial distribution of T cells compared to myeloid cell populations. In this context, knockout of EGFL7 led to a significant increase in the terminal effector CD8+ T cell population within the glioma mass. These results suggest that EGFL7 not only influences the functionality of immune cells but also their infiltration into glioma tissue. To elucidate the underlying

molecular mechanism, we focused on the interactome of EGFL7 within the GME and observed a strong interaction of EGFL7 with ITGB2, an immune cell receptor. In addition, we also found other interacting partners of EGFL7 within the GME, including ITGB1 and ITGAV, which are expressed on multiple cell types including endothelial cells, fibroblasts, glia cells and astrocytes, besides immune cells[38]. We focused on the ITGB2 protein motivated by its well-documented role in immune cell trafficking[31,39] and emerging evidence of its involvement in modulating immune cell functions in various tumor entities[29], including glioblastoma[40,41]. Moreover, the functions of EGFL7 through its interaction with ITGAV and enhancement of ITGB1 have already been reported in promoting angiogenesis[21,30].

In vitro analyses revealed that EGFL7 strongly affects the migration capacity of T cells in comparison to the myeloid population. Interestingly, this phenotype is exacerbated when ITGB2 is inhibited. Recent reports have shown that ITGB2 is highly expressed on anti-inflammatory macrophages and exhausted T cells[29]. The authors further observed that conformational inhibition of ITGB2 led to a decrease in anti-inflammatory macrophages and reduced the exhaustion of T cells in solid tumors such as colorectal cancer, pancreatic ductal adenocarcinoma and non-small cell lung cancer[29]. In this context, we also observed that ITGB2 deletion markedly reduced exhausted T cell frequencies, even in presence of ectopic mEGFL7 expression. Interestingly, ITGB2 deletion did not significantly alter the proportion of exhausted T cells in GL261-DsRed implanted mice. In contrast, ectopic EGFL7 expression - and its interaction with ITGB2 – appears to impact both immune cell migration and T cell exhaustion.

While our results are robust across multiple experimental platforms, regulatory T cells remain a challenge and warrant further investigation in follow-up studies. We observed discrepancies between single-cell transcriptomics and protein-level validation in our knockout model, which may arise from compensatory mechanisms triggered by the absence of EGFL7[43]. For instance, proteins such as VEGFA may get upregulated and contribute to increased infiltration of regulatory T cells within the tumor microenvironment[44]. These findings underscore the inherent complexity of immune profiling in brain tumors and highlight the necessity of multimodal validation approaches.

Together with previous findings[29], these observations show that the EGFL7-ITGB2 axis contributes to immunosuppression by impeding immune cell migration within the GME. Thus, the EGFL7–ITGB2 axis represents an attractive therapeutic target but direct inhibition of ITGB2 may inadvertently impair immune cells essential for anti-tumor immunity[34]. Consequently, we explored an alternative strategy to alleviate T cell exhaustion using anti-PD1 therapy[45].

We evaluated a combinatorial therapeutic strategy combining EGFL7 inhibition with PD1 immune checkpoint blockade. Strikingly, dual targeting led to a significant improvement in survival and delayed tumor progression compared to monotherapies. These findings further underscore the

potential of EGFL7 as a therapeutic target to enhance the efficacy of existing immunotherapies for glioma. Moreover, given that EGFL7 is a secreted protein, it may also serve as a viable biomarker or target for antibody- or peptide-based inhibition strategies[46].

Our results led us to propose a model wherein we aim to summarize our findings and introduce EGFL7 as a connecting link between angiogenesis and immunosuppression in glioblastoma (Figure 7). We have previously shown that EGFL7 promotes blood vessel formation and maturation in glioblastoma, which is favorable for the tumor microenvironment[21]. We believe that the angiogenic protein EGFL7, secreted into the GME, causes the recruitment of different immune cell populations including M2-like macrophages such as hypoxia-associated macrophages, lipid-associated macrophages along with MDSCs, through its interaction with ITGB2. Several reports have suggested that these myeloid populations promote angiogenesis through secretion of angiogenic factors such as vascular endothelial growth factor A (VEGFA), hypoxia-inducible factor 1 alpha or hexokinase-1[47]. Thus, on being recruited within the tumor microenvironment, these macrophages release angiogenic factors, which initiate a positive feedback loop for angiogenesis. This in turn causes increased secretion of EGFL7 from the endothelial cells of blood vessels followed by more recruitment of pro-tumorigenic M2-like macrophages along with increased exhaustion of CD8+ T cells (Figure 7). Eventually, with high levels of EGFL7, consequent increase in angiogenesis and immunosuppression lead to aggressive tumor growth. Thus, targeting EGFL7 along with PD1 inhibition may prove beneficial in the clinical context for treating glioblastoma patients, not only to reduce glioma-associated angiogenesis but also for curbing immunosuppression.

Our study delineates the role of EGFL7 in promoting immune evasion in glioblastoma and positions it alongside other angiogenic factors, such as VEGFA, that contribute to the tumor's immunosuppressive microenvironment[48]. VEGFA has been shown to promote differentiation of MDSCs and consequently the secretion of TGF-β1 by MDSCs, both known drivers of immunosuppression. Collagen-binding glycoprotein YKL-40 encoded by CHI3L1 gene is another angiogenic factor implicated in inducing immunosuppression in multiple cancers including lung, breast and skin cancer, besides glioblastoma[49]. It gets upregulated upon VEGFA inhibition especially in bevacizumab-resistant glioblastoma cells and inhibits CD8+ T cell recruitment[50]. Thus, targeting angiogenic factors which might have immunosuppressive capacities, along with immune checkpoint inhibition may prove beneficial in glioblastoma treatment as it would involve curbing angiogenesis mediated immune evasion.

In summary, we discovered that EGFL7 drives immunosuppression in glioblastoma by modulating the infiltration of myeloid and lymphoid cells. Its expression is associated with an increased percentage of M2-like immunosuppressive macrophages, MDSCs and T cell exhaustion along with a decline in M1-like pro-inflammatory macrophages. We further established that EGFL7 functions as an

immunosuppressive factor through its interaction with ITGB2. Targeting the EGFL7-ITGB2 axis – particularly in combination with immune checkpoint inhibitors – offers a promising strategy to reprogram the glioma immune microenvironment and improve patient outcomes. These findings provide a robust foundation for future translational studies aimed at incorporating EGFL7 blockade into the immunotherapeutic arsenal against glioblastoma.

Conflict of interest

The authors declare that there are no conflicts of interest.

Acknowledgements

Funded by the Deutsche Forschungsgemeinschaft (DFG, German Research Foundation) – Project-ID 318346496 – SFB 1292, project TP09 (M.H.H.S.)

Material and methods:

Cell culture:

Mouse glioma cells GL261 and SB28 were cultured in Dulbecco's modified Eagle's medium (DMEM, #41966029; Thermo Fisher Scientific, Waltham, MA, USA) supplemented with 10% fetal calf serum (Thermo) plus penicillin/streptomycin (Thermo). HEK293-EBNA cells were cultured in DMEM (#41965039, Thermo) supplemented with 10% fetal calf serum (Thermo) plus geneticin (#10131035, Thermo). Cells were cultured at 37 °C and 5% CO_2.

Murine immune cell sorting for migration assay

C57BL/6 mice were euthanized by administering a mixture of ketamine-xylazine intraperitoneally [ketamine 450 mg/kg, xylazine 48 mg/kg mixed in 0.9% sodium chloride solution], followed by transcardial perfusion with phosphate-buffered saline (PBS). Immune cells were isolated from spleen by dissociation in HBSS using the gentleMACS™ Octo Dissociator, employing the pre-set neural tissue dissociation kit (NTDK) program at 37 °C. After dissociation, cells were rinsed with HBSS and passed through a 70-µm cell strainer to achieve a single-cell suspension, yielding approximately 25 million cells. CD45+ immune cells were sorted using magnetic-activated cell sorting (MACS) according to the manufacturer's instructions (Mouse CD45+ microbeads, # 130-052-301, Miltenyi Biotec).

Murine pan T cell sorting for exhaustion assay

C57BL/6 mice were euthanized by administering an overdose of ketamine-xylazine mixture intraperitoneally [ketamine 450 mg/kg, xylazine 48 mg/kg mixed in 0.9% sodium chloride solution],

followed by transcardial perfusion with phosphate-buffered saline (PBS). T cells were isolated from spleen in HBSS solution using the gentleMACS™ Octo Dissociator, employing the pre-set neural tissue dissociation kit (NTDK) program at 37 °C.. Afterwards, cells were rinsed with HBSS and passed through a 40-µm cell strainer to achieve a single-cell suspension. T cells were sorted using the Pan T cell isolation kit II according to the manufacturer's instructions (Miltenyi Biotec). 96-wells were coated with CD3/CD28 antibodies for 4 hours at 37 °C for stimulating T cells. Accordingly, 1.5 x 10^5 cells were seeded in each 96-well for different conditions described in Figure 2G. Cells were incubated with different concentrations (1, 2 and 5 µg/ml) of purified murine EGFL7 protein to study the impact of EGFL7 on T cell exhaustion. After 5 days of incubation at 37 °C, cells were stained for different T cell markers and analyzed using a Symphony A3 system (BD Biosciences).

Protein purification:

Recombinant mouse EGFL7 protein was expressed in Sf9 cells using a baculovirus system as described previously[51]. Five days post-infection, cells were lysed in a pH 7.4 buffer containing Na□HPO□·2H□O, NaCl, Triton X-100, Leupeptin, Aprotinin, and PMSF using a glass homogenizer. Lysates were clarified by centrifugation, then treated with an SDS buffer (pH 10) comprising Na□HPO□·2H□O, NaCl, and SDS, followed by sonication (7 × 30 seconds). The HisTrap FF 5 ml column was equilibrated with equilibration buffer (pH 8.5) before sample loading. After collecting flow-through and a washing step, the bound protein was eluted with elution buffer (pH 8.5). Protein-containing fractions were pooled and dialyzed overnight against dialysis buffer (pH 8.5).

Migration assay:

CD45+ cells were isolated from the spleens of C57BL/6 mice using MACS and resuspended in serum free RPMI 1640 medium. Cells were counted using a hemocytometer. Transwell inserts (8 µm pore size) were placed in each well of a 24-well plate. 1 x 10^6 cells were incubated with the recombinant EGFL7, anti-ITGB2 antibody or both for 15 minutes at room temperature. Cells were seeded into transwell inserts in a 24-well plate. Plates were incubated at 37 °C for 1 hour and cells migrating to the lower chamber counted using Leica Microscope at 10x magnification.

Retroviral transduction:

Retroviral particles were produced in HEK293-EBNA cells by co-transfecting the plasmid of interest with the viral core packaging construct pUMVC and the envelope protein vector pCMV-VSV-G, as previously described[52]. The supernatant, which contained the viral particles, was used to transduce GL261 or SB28 cells. Successful gene transduction with either RV-C207-CAG-dsRedExpress2-WPRE or RV-C207-dsRed-mEGFL7 was visualized by the encoded DsRed. Transduced cells were isolated in a single sort using FACS Aria II (Becton Dickinson) device at the flow cytometry facility of the Institute for Physiological Chemistry, Dresden, Germany.

Immunoprecipitation:

The anti-V5 tag antibody (Abcam, ab27671; 1 µg per 1 mg of total protein) was used for co-immunoprecipitation, and the precipitated proteins on magnetic beads were subsequently analyzed by mass spectrometry. For *in vitro* validation studies, the following primary antibodies were used: mouse anti-Flag M2 (F3165, 1:2500, Sigma) and mouse anti-V5 tag (ab27671, 1:2500, Abcam). For western blotting, the following primary antibodies were used: anti-Flag tag antibody (20543-1-AP, 1:8000, Proteintech), mouse anti-V5 tag (ab27671, 1:2500, Abcam), anti-Myc tag (ab32072, 1:1000, Abcam), rabbit anti□β-actin (926-42210, 1:1000, Li-Cor). Secondary antibodies used: fluorescently labeled donkey-anti□rabbit (1:15,000, LI-COR Biosciences, Lincoln, NV, USA), fluorescently labeled Goat□anti□mouse (1:15,000, LI-COR Biosciences).

Mass spectrometry:

Co-immunoprecipitated proteins bound to dynabeads (Invitrogen) were processed for mass spectrometry analysis. Briefly, bead-bound proteins were washed three times with wash buffer (50 mM Tris-HCl, 50mM Tris-HCl, 150 mM NaCl, 1mM EDTA, 10% v/v Glycerol, 1% v/v Triton-X). Protein bound beads were resuspended in 2x S-TRAP buffer and 1x wash buffer. For analysis, 17 µl of the sample were injected into the HPLC system. A trap column was used to load the peptide mixture. It was desalted for 10 min with 0.1% formic acid (solvent A) at a flow rate of 3 µl/min. After desalting, the trap column was switched in-line with the separation column, operated at a flow rate of 200nl/min. Following equilibration with solvent A, peptides were separated in a linear gradient of 90 min from 0% - 60% solvent B (60% acetonitrile, 0.1% formic acid). The mass spectrometer (Q-Exactive HF, ThermoScientific, Bremen, Germany) was operated in data-dependent (DDA) acquisition mode. Peptide and protein identification was performed with Mascot V3.1.0 (Matrixscience), using the database of mouse reviewed proteins.

Animal models:

Animal experiments were approved by the ethics committee of TU Dresden and conducted according to the German Animal Protection Act. The experiment procedure was authorized by the Dresden Regional Council (Approval No. 25-5131/522/32 and 25-5131/542/35). All mice were housed in pathogen-free conditions with a 12-hour light-dark cycle and free access to food and water, at the experimental center of the Medical Theoretical Center (MTZ, Medical Faculty Carl Gustav Carus, Dresden, Germany).

Mouse lines:

C57BL/6J inbred mice (wildtype control mice) were purchased from Janvier Labs (Le Genest-Saint-Isle, France).

EGFL7 fl/fl;EIIa-Cre: Constitutive EGFL7 knockout (KO) mice were generated in our laboratory as previously described[54]. The *EGFL7* KO (EGFL7-/-) model was applied in tumor studies as a loss-of-function model. Their littermates (EGFL7+/+) were used as controls.

ITGB2 fl/fl;Scl-CreERT. Conditional ITGB2 fl/fl mice were provided by Stephan Grabbe (Institute of Dermatology, Johannes Gutenberg University Mainz, Mainz, Germany). In these mice, exon 3 of the *Itgb2* gene was flanked by loxP sites[53]. They were crossed with Scl-CreERT mice[54], which express a Cre/ERT fusion gene under the control of the stem cell enhancer and the 6E5 stem cell leukemia (Scl) exon 4 promoter, allowing the tamoxifen-induced deletion of ITGB2 in hematopoietic stem cells that give rise to all immune cells. Scl-CreERT mice were provided by Tatyana Grinenko (Institute of Molecular Medicine, Shanghai, China) and originated from Joachim Göthert's group (University Hospital Essen, Essen, Germany). At five weeks of age, *ITGB2 fl/fl;Scl-CreERT* mice were administered tamoxifen to induce Cre-mediated deletion of ITGB2 in hematopoietic stem cells, which give rise to immune cells. Following an 8-week period to allow mature ITGB2-deficient immune cells to repopulate secondary lymphoid organs.

NSG. The immune-compromised NOD/SCID/IL2rγ^{null} (NSG) mice[55] were provided by Kurt Reifenberg (DKFZ, Heidelberg, Germany) and originated from Charles River Laboratories, JAX stock #005557 (Sulzfeld, Germany).

Intracranial tumor implantations:

For stereotactic intracranial injections, 8-10 weeks old mice were anesthetized prior to intracranial implantation using 2% isoflurane (Primal). The anesthetized mice were fixed in a stereotactic frame and the anesthesia maintained via a nose cone adapter. A hole was drilled through the skull at the following coordinates relative to the bregma: 0.5 mm anterio-posterior and 2 mm medio-lateral. 2.5 x 10^4 GL261 cells or 1000 SB28 cells were injected 3.5 mm dorso-ventral of the dura mater into the striatum of different mice strains. Carprofen was administered as an analgesic at 10 mg/kg bodyweight subcutaneously before surgery. The care and euthanasia of the mice were carried out in accordance with the German Animal Welfare Act and approved by the Ethics committee of TU Dresden.

Mice were euthanized by administering an overdose of ketamine-xylazine mixture intraperitoneally [ketamine 450 mg/kg, xylazine 48 mg/kg mixed in 0.9% sodium chloride solution],

and the tumor tissue was processed for flow cytometry experiments. Alternatively, mice were sacrificed by transcardial perfusion using 4% PFA solution after 28 days or upon the development of GBM-specific symptoms, such as weight loss, difficulty in movement and disheveled fur, for flow cytometry.

Treatment experiments:

For treatment experiments, glioma-bearing mice received intraperitoneal injections of an isotype control antibody (10 mg per kg body weight (mpk) IgG2b, 10 mpk anti-EGFL7-blocking antibody (Genetech), 10 mpk anti-PD1-blocking antibody, or both anti-EGFL7-blocking and anti-PD1-blocking antibodies once every five days post two weeks of intracranial tumor engraftment.

Tamoxifen administration:

Tamoxifen (TAM) was administered to inducible mouse models to activate Cre-mediated recombination and knock out genes of interest. In *ITGB2 fl/fl;Scl-CreERT* mice, TAM (150 mpk) was injected intraperitoneally for three consecutive days at 4 and and 5 weeks of age. Tumor engraftment was performed 8 weeks post TAM administration.

Tissue preparation for immunohistochemistry:

Mice were anesthetized by administering a mixture of ketamine-xylazine intraperitoneally [ketamine 450 mg/kg, xylazine 48 mg/kg mixed in 0.9% sodium chloride solution], followed by transcardial perfusion with phosphate-buffered saline (PBS) and 4% paraformaldehyde (4% PFA). The brains were removed, fixed in 4% PFA at 4 °C for 24 hours. Finally, glioma-bearing brains were embedded in paraffin and 5 µm thick sections were prepared using microtome (RM2065, Leica).

Flow cytometry:

Mice were sacrificed by administering an overdose of ketamine-xylazine as described above. Following transcardial perfusion with 1 x HBBS, brains were removed and tumor tissue excised. The tumor tissue was resuspended in an enzyme mixture containing collagenase D, DNase, trypsin inhibitor and HEPES. Following neural tissue dissociation protocol for 22 minutes of dissociation in the Octo MACS dissociator, cells were passed through 70 µm strainer. Single cell suspension underwent debris removal using the kit from Miltenyi Biotec.

Cells were incubated on ice for 10 minutes in a solution containing rat anti-mouse CD16/CD32 (at a concentration of 1:200) and Zombie aqua fixable live-dead dye (concentration of 1:1000). After washing with FACS buffer and centrifugation, cells were stained.

Extracellular staining was performed for T cells using fluorochrome-labeled antibodies to mouse CD45 (#568336, 1:300, BD), CD3 (#749277, 1:100, BD), CD8a (#565968, 1:100, BD), CD4 (#100405, 1:200, Biolegend), CD25 (#101915, 1:100, Biolegend), Ly6C (#563011,1:300, BD), CD279 (#752354, 1:200, BD). For intracellular staining, cells were fixed/permeabilized according to the manufacturer's instructions. Immunostaining was done with the following antibodies: GATA-3 (#563349, 1:400), INFγ (#564336, 1:400), Tbet (#564141, 1:250), Granzyme B (#570498, 1:100), FoxP3 (#563486, 1:200) and Rorγt (#567362, 1:200, all obtained from BD).

Similarly, extracellular staining for myeloid cell populations was performed using fluorochrome-labeled antibodies to mouse CD45 (#568336, 1:300, BD), CD11b (#563553, 1:100, BD Horizon), CD11c (#566505, 1:200, BD Horizon), I-A/I-E (MHC-Class II; #107643, 1:200, Biolegend), CD80 (#562611, 1:200, BD), CD206 (#141723, 1:200, Biolegend), GR-1 (#108440, 1:300,Biolegend), CD170 (#155507, 1:80, Biolegend), TMEM119 (#25-6119-82, 1:200, Invitrogen) and F4/80 (#123141, 1:200, Biolegend). For intracellular staining, cells were fixed/permeabilized according to the manufacturer's instructions. Immunostaining was done with the following antibodies: Arginase (#53-3697-82, 1:200, Invitrogen) and iNOS (#696807, 1:100, Biolegend).

All stained samples were recorded using Symphony A3 (Becton Dickinson) device at the flow cytometry facility of the Institute of Physiological Chemistry, Dresden, Germany and analyzed with FlowJo software.

Isolation of immune cells for scRNA-sequencing

Glioma bearing mice were anesthetized and transcardially perfused with 20 ml of ice-cold 1 x HBSS. The brains were collected and tumors carefully excised using a stereomicroscope to avoid contamination with healthy brain tissue. Tumor samples were cut into small pieces and added into an enzyme mix containing collagenase D, pancreatic DNase, Trypsin inhibitor, Anisomycin, diluted in water and HEPES. Following 22 min of dissociation at 37 °C using Octo MACS dissociator, C-tubes were centrifuged and enzyme reaction stopped by adding ice cold 1 x HBSS. Tumor tissue was finally crushed with a syringe plunger and cells filtered through a 70 µm strainer. Following centrifugation at 500 x g for 10 minutes at 4 °C, the supernatant was removed, and the cell pellet was resuspended in 3.1 ml PBS and 0.9 ml debris removal solution. The solution was overlayed with 4 ml of PBS added dropwise on the side of the 15 ml tube tilted at a 45 degrees angle. Sample was centrifuged for 10 minutes at 3000 x g at 4 °C following which cell pellet was washed with 1 x PBS. Cells were resuspended in solution containing 10 µl of CD45+ microbeads and 90 µl MACS buffer (0.5 % BSA, 2 mM EDTA dissolved in 1 x PBS) and incubated for 15 minutes at 4 °C in dark. CD45+ cells were sorted using MS columns and the previous step repeated to increase the enrichment of CD45 expressing cells. After cell counting, samples were fixed/permeabilized using 10x permeabilization kit (Conc. Fix & Perm Buffer B) and kept at 4 °C for 16-24 hours. Following

centrifugation, the supernatant was removed, and cells were resuspended in a solution of glycerol and quenching buffer. All samples were stored at -80 °C until further processing at the Dresden Genome Center, CRTD, Dresden, Germany.

Processing scRNA-seq data

To build the reference for Cell Ranger, mouse (*Mus musculus*) genome (GRCm39) as well as gene annotation were downloaded from Ensembl release 104. The annotation was filtered with the 'mkgtf' command of Cell Ranger (options: '–attribute=gene_biotype:protein_coding –attribute=gene_biotype: lincRNA –attribute=gene_biotype:antisense'). Genome sequence and filtered annotation were then used as input to the 'mkref' command of Cell Ranger to build the appropriate Cell Ranger Reference. The raw sequencing data was then processed with the 'count' command of the Cell Ranger software (v7.1.0) provided by 10× Genomics.

For clustering and gene expression analysis, we used Seurat v.5.0.1 and the following analysis pipeline: Barcodes (cells) are kept unfiltered, features (genes) are filtered for having at least 10 cells with at least 1 read. The raw data as UMI counts were regressed to remove the effect of library size using single-cell transform (sct). Highly variable genes were identified using the variance-stabilizing transformation (vst), selecting the top 3,000. These genes were scaled and used as input for the dimensionality reduction by PCA analysis. A total of 50 principal components were calculated and the top 20 used for further calculations. For visualization purposes, Uniform Manifold Approximation and Projection (UMAP, k nearest neighbors = 30) was applied to project high-dimensional gene expression data into two dimensions. Graph-based clustering (k nearest neighbors = 30, resolution = 0.5) uses the Leiden algorithm[56]. Marker genes that are differentially expressed for each cluster (DEGs) are identified using the Wilcoxon rank-sum test and Benjamini-Hochberg method to correct for multiple comparisons (presto v1.0.0). DEGs which are expressed in at least 25% of the cells in a cluster and with a log2 fold change >1 were included.

Tissue processing and sample preparation

Brains from GL261 tumor-bearing EGFL7+/+ and EGFL7-/- mice were snap-frozen in isopentane, embedded in pre-chilled optimal cutting temperature compound (OCT) (Tissue-Tek O.C.T. Compound, SAKURA), and then cryosectioned into 10 μm sections at −20 °C. Brain sections with obvious tumor areas were collected.

Spatial transcriptomics processing

Spatial transcriptomic profiling was performed using the 10x Genomics Visium Spatial Gene Expression platform according to the manufacturer's protocol. 10 μm brain sections were placed onto Visium slides containing spatially barcoded capture areas, then subsequently fixed and stained

with H&E. Sections were imaged to capture tissue morphology and facilitate spatial mapping. Tissue permeabilization was optimized to release mRNA, which hybridized to spatially barcoded oligonucleotides on the capture spots. In situ reverse transcription was performed to generate cDNA incorporating unique molecular identifiers (UMIs) and spatial barcodes. Libraries were prepared by PCR amplification following the manufacturer's guidelines and sequenced on an Illumina platform. Sequencing reads were aligned to the reference genome, and spatial gene expression data were processed using the 10x Genomics Space Ranger software. Visualization and downstream analyses of spatial expression patterns were conducted using Loupe Browser and additional bioinformatics tools.

Magnetic resonance imaging (MRI)

A 7 Tesla ClinScan 70/30 small animal ultra-high-field MRI scanner equipped with a mouse whole-body coil (Bruker, Ettlingen, Germany) was used for assessing the tumor volume of glioma-bearing mice. The mice were anesthetized with 2% isoflurane mixed with oxygen, prior to imaging. A respiration monitor was used to ensure stable breathing along with a heated animal bed to maintain the body temperature. T2-weighted images were acquired with a repetition time of 2500 milliseconds (ms), an echo time of 33 ms and a slice thickness of 0.5 mm with no interslice gap. Tumor volumes were quantified using T2-weighted images analyzed with ImageJ software. Tumor area was averaged across the slices and multiplied by the thickness of the tissue to determine the volume of the tumor.

Statistics:

All data were analyzed using GraphPad Prism 6 software (GraphPadSoftware, La Jolla, CA, USA). Unless otherwise specified, the data are presented as mean ± standard error of mean (SEM) of three independent biological experiments while animal experiments were performed with a minimum of six mice per group. Statistical analysis was performed using one-way analysis of variance (ANOVA) for three or more groups followed by post hoc analysis, or the Mann–Whitney U-test for comparison of two groups. For survival analyses, Kaplan–Meier survival curves were generated and compared using the log-rank test. Sample size and statistical methods used in the analyses are described in figure legends.

References:

1. Nørøxe, D. S., Poulsen, H. S. & Lassen, U. Hallmarks of glioblastoma: A systematic review. *ESMO Open* vol. 1 Preprint at https://doi.org/10.1136/esmoopen-2016-000144 (2016).
2. van Solinge, T. S., Nieland, L., Chiocca, E. A. & Broekman, M. L. D. Advances in local therapy for glioblastoma — taking the fight to the tumour. *Nature Reviews Neurology* vol. 18 Preprint at https://doi.org/10.1038/s41582-022-00621-0 (2022).

3. Albini, A. & Sporn, M. B. The tumour microenvironment as a target for chemoprevention. *Nature Reviews Cancer* vol. 7 Preprint at https://doi.org/10.1038/nrc2067 (2007).

4. DeCordova, S. *et al.* Molecular Heterogeneity and Immunosuppressive Microenvironment in Glioblastoma. *Frontiers in Immunology* vol. 11 Preprint at https://doi.org/10.3389/fimmu.2020.01402 (2020).

5. Lee, J., Nicosia, M., Silver, D. & Lathia, J. Sex-specific T cell exhaustion drives differential immune responses in glioblastoma. *The Journal of Immunology* **210**, (2023).

6. Woroniecka, K. *et al.* T-cell exhaustion signatures vary with tumor type and are severe in glioblastoma. *Clinical Cancer Research* **24**, (2018).

7. Yeo, A. T. *et al.* Single-cell RNA sequencing reveals evolution of immune landscape during glioblastoma progression. *Nat Immunol* **23**, (2022).

8. Mahajan, S., Schmidt, M. H. H. & Schumann, U. The Glioma Immune Landscape: A Double-Edged Sword for Treatment Regimens. *Cancers* vol. 15 Preprint at https://doi.org/10.3390/cancers15072024 (2023).

9. Hotchkiss, K. M. *et al.* Dendritic cell vaccine trials in gliomas: Untangling the lines. *Neuro-Oncology* vol. 25 Preprint at https://doi.org/10.1093/neuonc/noad088 (2023).

10. Bagley, S. J., Desai, A. S., Linette, G. P., June, C. H. & O'Rourke, D. M. CAR T-cell therapy for glioblastoma: Recent clinical advances and future challenges. *Neuro Oncol* **20**, (2018).

11. Aslan, K. *et al.* Heterogeneity of response to immune checkpoint blockade in hypermutated experimental gliomas. *Nat Commun* **11**, (2020).

12. Rizvi, N. A. *et al.* Mutational landscape determines sensitivity to PD-1 blockade in non-small cell lung cancer. *Science (1979)* **348**, (2015).

13. Hugo, W. *et al.* Genomic and Transcriptomic Features of Response to Anti-PD-1 Therapy in Metastatic Melanoma. *Cell* **165**, (2016).

14. Ferris, R. L. *et al.* Nivolumab for Recurrent Squamous-Cell Carcinoma of the Head and Neck. *New England Journal of Medicine* **375**, (2016).

15. Reardon, D. A. & Weller, M. Vaccination for IDH-mutant tumors: A novel therapeutic approach applied to glioma. *Med* **2**, (2021).

16. Lim, M. *et al.* Phase III trial of chemoradiotherapy with temozolomide plus nivolumab or placebo for newly diagnosed glioblastoma with methylated MGMT promoter . *Neuro Oncol* **24**, 1935–1949 (2022).

17. Cloughesy, T. F. *et al.* Neoadjuvant anti-PD-1 immunotherapy promotes a survival benefit with intratumoral and systemic immune responses in recurrent glioblastoma. *Nat Med* **25**, (2019).

18. Ahluwalia, M. S. *et al.* Phase II trial of SurVaxM combined with standard therapy in patients with newly diagnosed glioblastoma. *Journal of Clinical Oncology* **36**, (2018).

19. Delfortrie, S. *et al.* Egfl7 promotes tumor escape from immunity by repressing endothelial cell activation. *Cancer Res* **71**, 7176–7186 (2011).

20. Pinte, S. *et al.* EGF repeats of epidermal growth factor-like domain 7 promote endothelial cell activation and tumor escape from the immune system. *Oncol Rep* **47**, (2022).

21. Dudvarski Stanković, N. *et al.* EGFL7 enhances surface expression of integrin α 5 β 1 to promote angiogenesis in malignant brain tumors . *EMBO Mol Med* **10**, (2018).

22. García-Vicente, L. *et al.* Single-nucleus RNA sequencing provides insights into the GL261-GSC syngeneic mouse model of glioblastoma. *bioRxiv* 2023.10.26.564166 (2023) doi:10.1101/2023.10.26.564166.

23. Pombo Antunes, A. R. *et al.* Single-cell profiling of myeloid cells in glioblastoma across species and disease stage reveals macrophage competition and specialization. *Nat Neurosci* **24**, (2021).

24. Governa, V. *et al. Protumoral Lipid Droplet-Loaded Macrophages Are Enriched in Human Glioblastoma and Can Be Therapeutically Targeted*. *Sci. Transl. Med* vol. 16 https://www.science.org (2024).

25. Pang, L., Zhou, F. & Chen, P. Lipid-Laden Macrophages Recycle Myelin to Feed Glioblastoma. *Cancer Res* **84**, 3712–3714 (2024).

26. Andreatta, M. *et al.* Interpretation of T cell states from single-cell transcriptomics data using reference atlases. *Nat Commun* **12**, (2021).

27. Eden, E., Navon, R., Steinfeld, I., Lipson, D. & Yakhini, Z. GOrilla: A tool for discovery and visualization of enriched GO terms in ranked gene lists. *BMC Bioinformatics* **10**, (2009).

28. Shannon, P. *et al.* Cytoscape: A software Environment for integrated models of biomolecular interaction networks. *Genome Res* **13**, (2003).

29. Han, I.-H. *et al.* Conformation-sensitive targeting of CD18 depletes M2-like tumor-associated macrophages resulting in inhibition of solid tumor progression. *J Immunother Cancer* **13**, e011422 (2025).

30. Nikolić, I. *et al.* EGFL7 ligates αvβ3 integrin to enhance vessel formation. *Blood* **121**, (2013).

31. Walling, B. L. & Kim, M. LFA-1 in T cell migration and differentiation. *Frontiers in Immunology* vol. 9 Preprint at https://doi.org/10.3389/fimmu.2018.00952 (2018).

32. Xia, Y. *et al.* Function of the Lectin Domain of Mac-1/Complement Receptor Type 3 (CD11b/CD18) in Regulating Neutrophil Adhesion. *The Journal of Immunology* **169**, (2002).

33. Heit, B., Colarusso, P. & Kubes, P. Fundamentally different roles for LFA-1, Mac-1 and α 4-integrin in neutrophil chemotaxis. *J Cell Sci* **118**, (2005).

34. Haake, M. *et al.* Tumor-derived GDF-15 blocks LFA-1 dependent T cell recruitment and suppresses responses to anti-PD-1 treatment. *Nat Commun* **14**, (2023).

35. Reardon, D. A. *et al.* Effect of Nivolumab vs Bevacizumab in Patients with Recurrent Glioblastoma: The CheckMate 143 Phase 3 Randomized Clinical Trial. *JAMA Oncol* **6**, (2020).

36. Tong, N. *et al.* Tumor Associated Macrophages, as the Dominant Immune Cells, Are an Indispensable Target for Immunologically Cold Tumor—Glioma Therapy? *Frontiers in Cell and Developmental Biology* vol. 9 Preprint at https://doi.org/10.3389/fcell.2021.706286 (2021).

37. DeNardo, D. G. & Ruffell, B. Macrophages as regulators of tumour immunity and immunotherapy. *Nature Reviews Immunology* vol. 19 369–382 Preprint at https://doi.org/10.1038/s41577-019-0127-6 (2019).

38. Karlsson, M. *et al.* A single–cell type transcriptomics map of human tissues. *Sci Adv* **7**, (2021).

39. Shi, H. & Shao, B. LFA-1 Activation in T-Cell Migration and Immunological Synapse Formation. *Cells* vol. 12 Preprint at https://doi.org/10.3390/cells12081136 (2023).

40. Xu, H. *et al.* ITGB2 as a prognostic indicator and a predictive marker for immunotherapy in gliomas. *Cancer Immunology, Immunotherapy* **71**, (2022).

41. Liu, H. *et al.* Correlation between ITGB2 expression and clinical characterization of glioma and the prognostic significance of its methylation in low-grade glioma(LGG). *Front Endocrinol (Lausanne)* **13**, (2023).

42. Sai Krishna, A. V. S., Ramu, A., Hariharan, S., Sinha, S. & Donakonda, S. Characterization of tumor microenvironment in glioblastoma multiforme identifies ITGB2 as a key immune and stromal related regulator in glial cell types. *Comput Biol Med* **165**, (2023).

43. El-Brolosy, M. A. & Stainier, D. Y. R. Genetic compensation: A phenomenon in search of mechanisms. *PLoS Genetics* vol. 13 Preprint at https://doi.org/10.1371/journal.pgen.1006780 (2017).

44. Bourhis, M., Palle, J., Galy-Fauroux, I. & Terme, M. Direct and Indirect Modulation of T Cells by VEGF-A Counteracted by Anti-Angiogenic Treatment. *Frontiers in Immunology* vol. 12 Preprint at https://doi.org/10.3389/fimmu.2021.616837 (2021).

45. Xu, Y. *et al.* The roles of PD-1/PD-L1 in the prognosis and immunotherapy of prostate cancer. *Molecular Therapy* vol. 29 Preprint at https://doi.org/10.1016/j.ymthe.2021.04.029 (2021).

46. Fabian, C., Mahajan, S. & Schmidt, M. H. H. EGFL7: An emerging biomarker with great therapeutic potential. *Pharmacol Ther* **266**, 108764 (2025).

47. Wang, W. *et al.* Identification of hypoxic macrophages in glioblastoma with therapeutic potential for vasculature normalization. *Cancer Cell* **42**, 815-832.e12 (2024).

48. Tian, Y., Gao, X., Yang, X., Chen, S. & Ren, Y. VEGFA contributes to tumor property of glioblastoma cells by promoting differentiation of myeloid-derived suppressor cells. *BMC Cancer* **24**, (2024).

49. Holst, C. B. *et al.* Perspective: targeting VEGF-A and YKL-40 in glioblastoma–matter matters. *Cell Cycle* **20**, 702–715 (2021).

50. Luo, J. *et al.* Vascular Immune Evasion of Mesenchymal Glioblastoma Is Mediated by Interaction and Regulation of VE-Cadherin on PD-L1. *Cancers (Basel)* **15**, (2023).

51. Schmidt, M. H. H. *et al.* Epidermal growth factor-like domain 7 (EGFL7) modulates Notch signalling and affects neural stem cell renewal. *Nat Cell Biol* **11**, 873–880 (2009).

52. Soneoka, Y. *et al.* A transient three-plasmid expression system for the production of high titer retroviral vectors. *Nucleic Acids Research* vol. 23 Preprint at https://doi.org/10.1093/nar/23.4.628 (1995).

53. Klaus, T. *et al.* Impaired Treg-DC interactions contribute to autoimmunity in leukocyte adhesion deficiency type 1. *JCI Insight* **7**, (2022).

54. Göthert, J. R. *et al.* In vivo fate-tracing studies using the Scl stem cell enhancer: Embryonic hematopoietic stem cells significantly contribute to adult hematopoiesis. *Blood* **105**, (2005).

55. Shultz, L. D. *et al.* Human Lymphoid and Myeloid Cell Development in NOD/LtSz-scid IL2R γ null Mice Engrafted with Mobilized Human Hemopoietic Stem Cells . *The Journal of Immunology* **174**, (2005).

56. Traag, V. A., Waltman, L. & van Eck, N. J. From Louvain to Leiden: guaranteeing well-connected communities. *Sci Rep* **9**, (2019).

Figure legends

Figure 1: EGFL7 expression is associated with poor prognosis in glioblastoma

A: Analysis of glioma patient samples from TCGA. **B:** MRI scan of tumors 25 days after EGFL7 +/+ and EGFL7 -/- mice were intracranially implanted with GL261-DsRed cells (top). Kaplan-Meier survival curve for GL261-DsRed implanted mice showing prolonged survival in EGFL7 -/- mice compared to their littermate controls (bottom; n = 10, $p < 0.0001$, log-rank test) **C:** Kaplan-Meier survival curve for GL261-mEGFL7 implanted mice compared to GL261-DsRed (bottom; n=8, p = 0.0002, log-rank test.) **D:** MRI scan of tumors 28 days after C57BL/6J were intracranially implanted with GL261-DsRed or GL261-mEGFL7 tumor cells (top). Analysis of tumor volume from day 7 to day 28 in tumor-bearing C57BL/6J mice (bottom; n = 5, $p < 0.001$, two-way ANOVA). **E:** Kaplan-Meier survival curve for GL261-mEGFL7 implanted mice compared to GL261-DsRed (bottom; n = 7, p = 0.8123, log-rank test). **F:** MRI scan of tumors 28 days after immuno-deficient NSG mice were intracranially implanted with GL261-DsRed or GL261-mEGFL7 tumor cells (top). Analysis of tumor volume from day 7 to day 28 in tumor-bearing NSG mice (bottom; n = 5, p = NS, two-way ANOVA).

Figure 2: Single cell analysis of immune cell populations from the tumor tissue in murine glioblastoma models

A: Immune cells were isolated using magnetic-activated cell sorting (MACS) from tumor tissues of both mouse models and processed for single cell RNA-sequencing (top). After single cell RNA sequencing, CD45+ immune cells were broadly classified into myeloid and lymphoid clusters (bottom). **B**: The immune cell clusters were annotated based on Garcia et al. **C**: UMAP comparing macrophage (TAM1) and microglia (TAM2) clusters in DsRed and mEGFL7 tumor tissues. **D**: Stacked barplot comparing different macrophage clusters between DsRed and mEGFL7. **E**: UMAP depicting T cell subsets in DsRed and mEGFL7 tumor tissues. **F**: Stacked barplot comparing different

T cell clusters between DsRed and mEGFL7. **G**: Flow cytometry analysis of different myeloid populations in the gain-of-function study (n = 7 for studying M2-like (CD206+ Arginase+), M1-like (CD80+ iNOS+) and MDSCs (Gr1+ CD11b+), n = 8 for microglia ($CD11b^{high}$ $CD45^{low}$), t-test followed by post-hoc hypothesis). **H:** Flow cytometry analysis of different T cell populations in the gain-of-function study (n=6 for studying exahusted T cells (PD1+ CD8+) and Tregs (Foxp3+ CD25+ CD4+), t-test followed by post-hoc hypothesis). **I:** Schematic describing the experiment to determine the effect of EGFL7 on T cell exhaustion *in vitro* (left). Flow cytometry analysis of effector T cells from three independent T cell stimulation experiments (right; p = 0.0225 using t-test).

Figure 3: EGFL7 affects immune cell distribution within GME

A: Spatial clusters within the brain for identifying the localization of immune cells. **B:** Label transfer of different cells was performed based on annotations from Garcia Vicente et al 2023[22]. **C:** Representative images of M1-like, lipid-associated and hypoxia-associated macrophage distribution using spatial transcriptomics in glioma mass of EGFL7+/+ and EGFL7-/- mice (top). Predictive analysis of the distribution of these myeloid cell populations in the tumor core, shell and healthy brain (bottom). **D:** Representative images of CD4+ naïve, terminal effector CD8+ T cells and Treg distribution using spatial transcriptomics in glioma mass of EGFL7+/+ and EGFL7-/- mice (top). Predictive analysis of the distribution of these T cell populations in the tumor core, shell and healthy brain (bottom). **E:** Histological analysis of different T cell populations (left to right: CD8+, CD4+, Foxp3+ cells per 2500 μm^2) in the glioma mass of EGFL7+/+ and EGFL7-/- mice (n = 5, non-parametric t test followed with post-hoc hypothesis testing).

Figure 4: EGFL7 interacts with immune cell specific receptor ITGB2 within the GME

A: Schematic for interactome analysis by mass spectrometry. V5-tagged EGFL7 was pulled down using an anti-V5 antibody. **B:** Gene Ontology analysis of proteins from the EGFL7 interactome. **C:** Bar plot showing abundance of different proteins in the EGFL7 interactome. Schematic of most abundant proteins interacting with EGFL7 in the tumor microenvironment. **D:** Vectors expressing V5-tagged β-integrins, Flag-tagged DsRed and EGFL7 were transfected in HEK293-EBNA cells (left). β-integrins tagged to V5 were pulled down using an anti-V5 antibody. Immunoblotting was performed using an anti-V5 antibody to capture the protein expression of β-integrins and an anti-Flag antibody for determining the abundance of Flag tagged EGFL7 and DsRed protein (right). **E:** Vectors expressing V5-tagged β-integrins, Flag-tagged DsRed and EGFL7 and Myc-tagged α-integrins were transfected in HEK293-EBNA cells. DsRed and EGFL7 tagged to Flag tag were pulled down using anti-Flag antibody. Immunoblotting was performed using anti-Flag antibody to capture the expression of β-integrins, anti-Myc antibody for observing Myc-tagged α-integrin expression and anti-Flag antibody for determining the expression of Flag-tagged EGFL7 and DsRed.

Figure 5: EGFL7 – ITGB2 interaction influences the migration of immune cells in vitro and T cell exhaustion in vivo

A: Statistical analysis of migration assay to determine the effect of EGFL7 on immune cell migration in vitro. control vs CCL2 (p = 0.0069) and CCL2 vs EGFL7 (p < 0.0001) **B:** Statistical analysis of migration assay to determine EGFL7 and abITGB2 effect on immune cell migration in vitro. p < 0.0001 (control vs CCL2, CCL2 vs EGFL7, CCL2 vs abITGB2, CCL2 vs EGFL7 + abITGB2) **C:** Statistical analysis of migration assay to determine EGFL7 and abITGB2 effect on myeloid cell migration in vitro. CCL2 vs EGFL7 (p = 0.0161), CCL2 vs abITGB2 (p = 0.0626), CCL2 vs EGFL7 + abITGB2 (0.0002) **D**. Statistical analysis of migration assay to determine EGFL7 and abITGB2 effect on T cell migration in vitro. p < 0.0001 (CCL2 vs EGFL7, CCL2 vs abITGB2, CCL2 vs EGFL7 + abITGB2) **E:** Kaplan-Meier survival curve for ITGB2 fl/fl and $ITGB2^{\Delta HSC}$ mice implanted with GL261-DsRed tumor cells. **F:** Analysis of tumor volume from day 7 to day 28 in GL261-DsRed implanted ITGB2 fl/fl and $ITGB2^{\Delta HSC}$ mice. **G:** Kaplan-Meier survival curve for ITGB2 fl/fl and $ITGB2^{\Delta HSC}$ mice implanted with GL261-mEGFL7 tumor cells. **H:** Analysis of tumor volume from day 7 to day 28 in GL261-mEGFL7 implanted ITGB2 fl/fl and $ITGB2^{\Delta HSC}$ mice. **I:** Flow cytometry

analysis of exhausted T cells from tumor tissues of ITGB2 fl/fl; Scl-Cre mice (n = 7) **J**: Flow cytometry analysis of hypoxia associated macrophages from tumor tissues of ITGB2 fl/fl; Scl-Cre mice (n = 5)

Figure 6: EGFL7 influences survival of tumor-bearing mice in an immune-dependent manner

A: Experimental design of GL261-tumor bearing mice treated with IgG control, anti-EGFL7, anti-PD1 monotherapy or anti-EGFL7 and anti-PD1 therapy on three separate days (day 16, 21 and 26). **B:** MRI scan of intracranially implanted GL261-DsRed mice on day 28 post TIMP (top), Kaplan-Meier survival analysis of mice intracranially implanted with GL261-DsRed cells and treated with blocking antibodies (bottom) (n=8 for IgG, anti-EGFL7 and anti-PD1, n=10 for anti-EGFL7 and anti-PD1). Statistical analysis showed significant difference in the survival between IgG, anti-EGFL7 and anti-PD1 therapy vs combinatorial anti-EGFL7 and anti-PD1 therapy with p = 0.0014, 0.0002 and 0.0001, respectively using log-rank test. **C:** MRI scan of intracranially implanted GL261-mEGFL7 mice on day 28 post TIMP (top), Kaplan-Meier survival analysis of mice intracranially implanted with GL261-mEGFL7 cells and treated with blocking antibodies (bottom) (n=8 for IgG, anti-EGFL7 and anti-PD1, n=10 for anti-EGFL7 and anti-PD1). Statistical analysis showed significant difference in the survival between IgG, anti-EGFL7 and anti-PD1 therapy vs combinatorial anti-EGFL7 and anti-PD1 therapy with p = 0.0003, 0.0011, and 0.0006, respectively using log-rank test.

Figure 7: EGFL7 promotes an immunosuppressive microenvironment by recruiting pro-tumorigenic macrophages and causing T cell exhaustion through its interaction with ITGB2

Extended Data:

Extended Data Fig 1: EGFL7 affects survival in glioblastoma

a: Schematic for gain-of-function and loss-of-function models. **b:** Immunostaining collagen IV (positive control for extracellular matrix) and V5 protein-tagged EGFL7 in the murine glioma tissue compared to negative control (DsRed). Collagen type IV is specifically expressed in the ECM. **c:** Kaplan-Meier survival curve shows EGFL7-/- mice intracranially implanted with SB28 cells survived longer compared to EGFL7+/+ mice (n = 9, p = 0.0038, log-rank test). **d:** Kaplan-Meier survival curve shows C57BL/6 mice intracranially implanted with SB28-mEGFL7 cells had a reduced survival compared to SB28-DsRed implanted mice (n=9 for EGFL7+/+ and n=7 for EGFL7-/- mice, p = 0.0196, log-rank test).

Extended Figure 2: scRNAseq analysis of immune cells from glioma mass of loss-of-function study

a: Dotplot showing differentially expressed genes in different myeloid cell clusters. **b:** UMAP depicting myeloid cell subsets in glioma tissue from EGFL7 +/+ and EGFL7 -/- mice. **c:** Stackplot showing the proportion of different myeloid cells in EGFL7+/+ and EGFL7-/- mice. **d:** Dotplot showing differentially expressed genes in different T cell clusters. **e:** UMAP depicting T cell subsets in glioma tissue from EGFL7+/+ and EGFL7-/- mice. **f:** Stackplot showing the proportion of different T cells in EGFL7+/+ and EGFL7-/- mice.

Extended Data Fig. 3: Validation of scRNA-seq data of loss-of-function study using flow cytometry analysis

a: Flow cytometry analysis of macrophages (F4/80+/CD11b+), MDSCs (Gr1+/CD11b+) and microglia ($CD11b^{high}/CD45^{low}$) (n = 5, p = 0.0162, 0.0176 for macrophages and MDSCs, respectively; microglial population was not significantly different between EGFL7+/+ and EGFL7-/- mice) **b:** Flow cytometry analysis of CD8+ T cells (CD8+/CD3+), effector T cells (Gzmb+/CD8+) and Tregs (CD25+ Foxp3+/CD4+) from tumor tissues of EGFL7+/+ and EGFL7-/- mice (n=5; p = 0.0011, 0.0159, 0.0191 for CD8+ T cells, effector T cells and Tregs respectively)

Extended Data Fig. 4: EGFL7 inhibits immune cell migration in vitro

a: Schematic showing splenocytes were isolated and CD45+ immune cells were sorted for transwell migration assay **b:** Schematic showing different conditions for testing effect of EGFL7 on immune cell migration (1: control medium, 2: Medium with chemoattractant CCL2, 3: Cell suspension supplemented with purified recombinant EGFL7, 4: Cell suspension supplemented with purified recombinant EGFL7 + medium containing CCL2. **c.** Representative images of transwell migration assay showing impact of EGFL7 on immune cell migration. **d.** Representative images of transwell migration assay showing impact of EGFL7 and abITGB2 on immune cell migration.

Figure 1

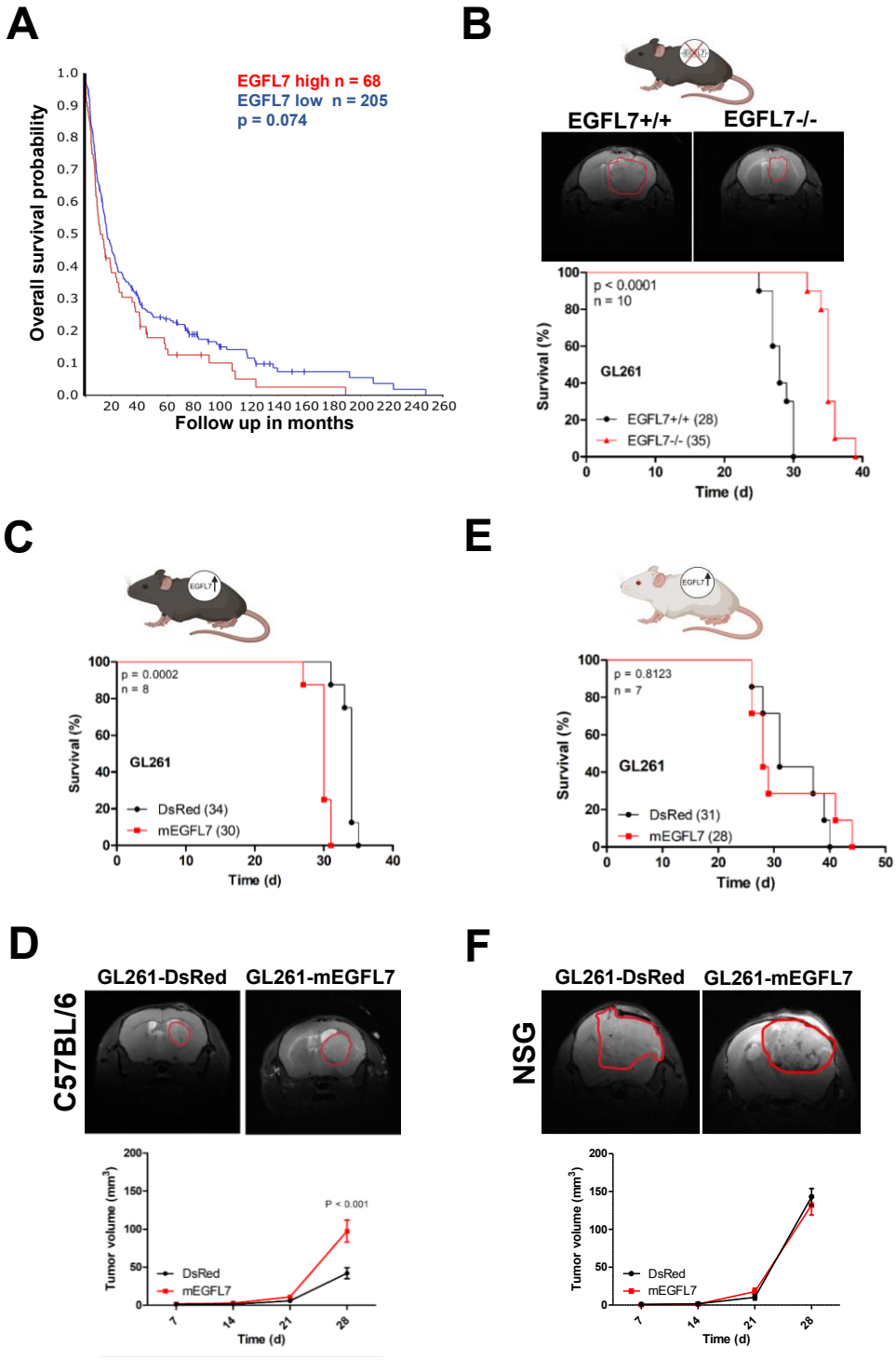
A
EGFL7 high n = 68
EGFL7 low n = 205
p = 0.074
Overall survival probability
Follow up in months
B
EGFL7+/+
EGFL7-/-
p < 0.0001
n = 10
GL261
EGFL7+/+ (28)
EGFL7-/- (35)
Survival (%)
Time (d)
C
p = 0.0002
n = 8
GL261
DsRed (34)
mEGFL7 (30)
Survival (%)
Time (d)
E
p = 0.8123
n = 7
GL261
DsRed (31)
mEGFL7 (28)
Survival (%)
Time (d)
D
C57BL/6
GL261-DsRed
GL261-mEGFL7
P < 0.001
DsRed
mEGFL7
Tumor volume (mm3)
Time (d)
F
NSG
GL261-DsRed
GL261-mEGFL7
DsRed
mEGFL7
Tumor volume (mm3)
Time (d)

Figure 2

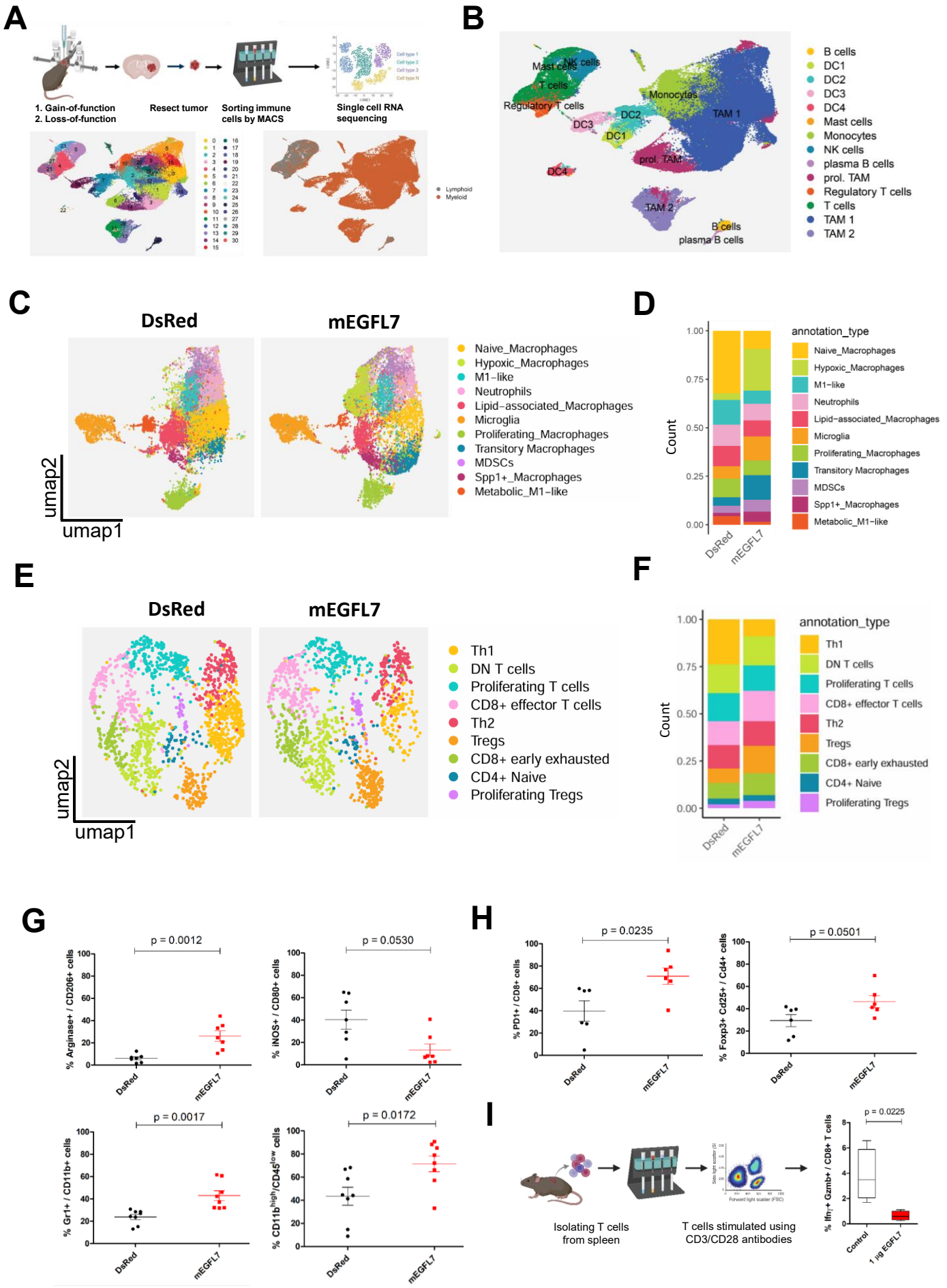
A
1. Gain-of-function
2. Loss-of-function
Resect tumor
Sorting immune cells by MACS
Single cell RNA sequencing
Lymphoid
Myeloid
B
Mast cells
NK cells
T cells
Regulatory T cells
Monocytes
DC2
DC3
DC1
TAM 1
prol. TAM
DC4
TAM 2
B cells
plasma B cells
B cells
DC1
DC2
DC3
DC4
Mast cells
Monocytes
NK cells
plasma B cells
prol. TAM
Regulatory T cells
T cells
TAM 1
TAM 2
C
DsRed
mEGFL7
umap2
umap1
Naive_Macrophages
Hypoxic_Macrophages
M1-like
Neutrophils
Lipid-associated_Macrophages
Microglia
Proliferating_Macrophages
Transitory Macrophages
MDSCs
Spp1+_Macrophages
Metabolic_M1-like
D
annotation_type
Count
1.00
0.75
0.50
0.25
0.00
DsRed
mEGFL7
Naive_Macrophages
Hypoxic_Macrophages
M1-like
Neutrophils
Lipid-associated_Macrophages
Microglia
Proliferating_Macrophages
Transitory Macrophages
MDSCs
Spp1+_Macrophages
Metabolic_M1-like
E
DsRed
mEGFL7
umap2
umap1
Th1
DN T cells
Proliferating T cells
CD8+ effector T cells
Th2
Tregs
CD8+ early exhausted
CD4+ Naive
Proliferating Tregs
F
annotation_type
Count
1.00
0.75
0.50
0.25
0.00
DsRed
mEGFL7
Th1
DN T cells
Proliferating T cells
CD8+ effector T cells
Th2
Tregs
CD8+ early exhausted
CD4+ Naive
Proliferating Tregs
G
p = 0.0012
% Arginase+ / CD206+ cells
p = 0.0530
% iNOS+ / CD80+ cells
p = 0.0017
% Gr1+ / CD11b+ cells
p = 0.0172
% CD11b^high/CD45^low cells
DsRed
mEGFL7
H
p = 0.0235
% PD1+ / CD8+ cells
p = 0.0501
% Foxp3+ Cd25+ / Cd4+ cells
DsRed
mEGFL7
I
Isolating T cells from spleen
T cells stimulated using CD3/CD28 antibodies
p = 0.0225
% Ifnγ+ Gzmb+ / CD8+ T cells
Control
1 µg EGFL7

Figure 3

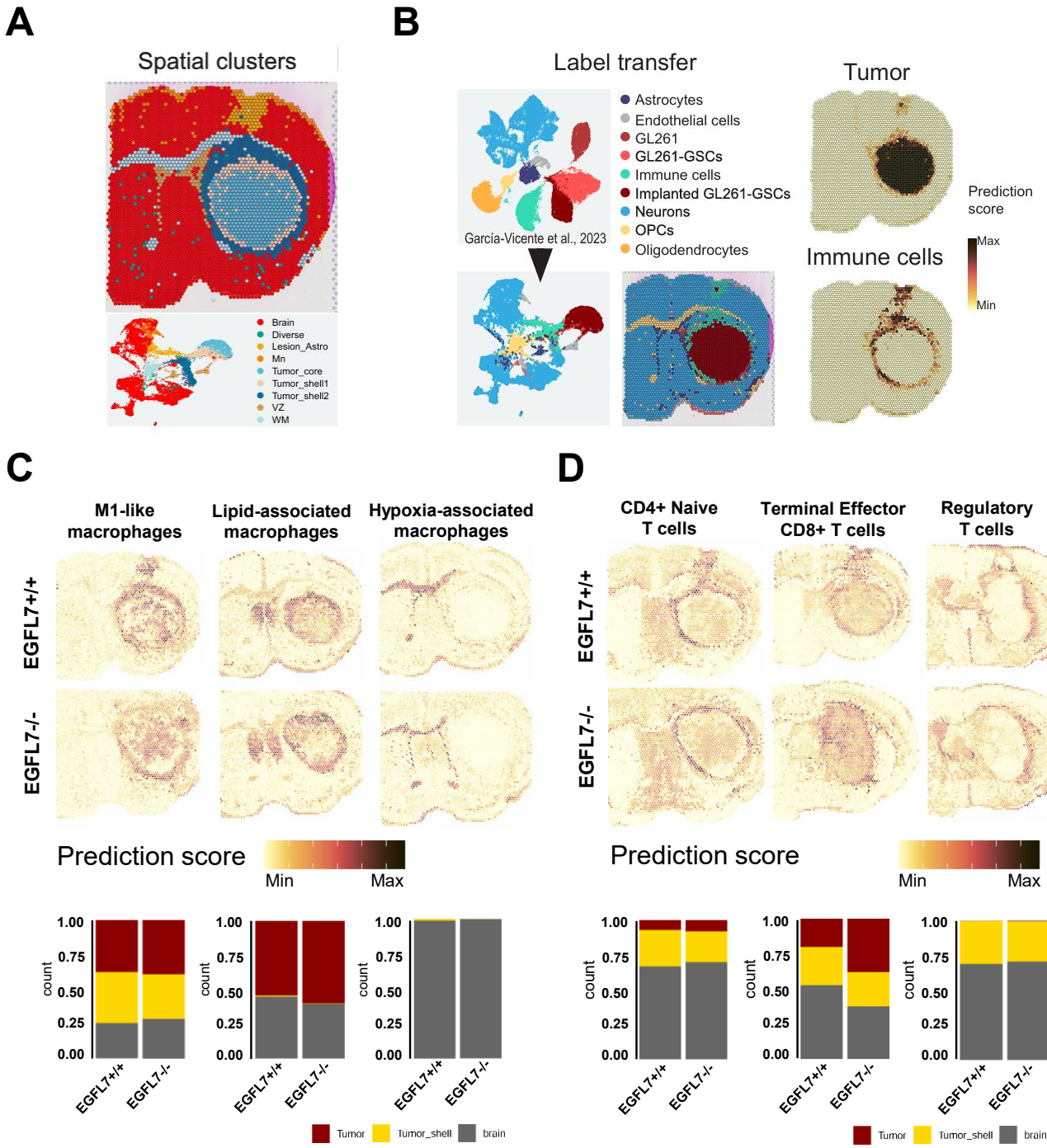
A
Spatial clusters
Brain
Diverse
Lesion_Astro
Mn
Tumor_core
Tumor_shell1
Tumor_shell2
VZ
WM
B
Label transfer
García-Vicente et al., 2023
Astrocytes
Endothelial cells
GL261
GL261-GSCs
Immune cells
Implanted GL261-GSCs
Neurons
OPCs
Oligodendrocytes
Tumor
Immune cells
Prediction score
Max
Min
C
M1-like macrophages
Lipid-associated macrophages
Hypoxia-associated macrophages
EGFL7+/+
EGFL7-/-
Prediction score
Min
Max
count
EGFL7+/+
EGFL7-/-
Tumor
Tumor_shell
brain
D
CD4+ Naive T cells
Terminal Effector CD8+ T cells
Regulatory T cells
EGFL7+/+
EGFL7-/-
Prediction score
Min
Max
count
EGFL7+/+
EGFL7-/-
Tumor
Tumor_shell
brain
E
EGFL7 +/+
EGFL7 -/-
p = 0.0003
CD8a+ cells / 2500 um2
Core
p < 0.001
CD4+ cells / 2500 µm2
Core
p = 0.0059
FoxP3+ cells / 2500 um2
Core

Figure 4

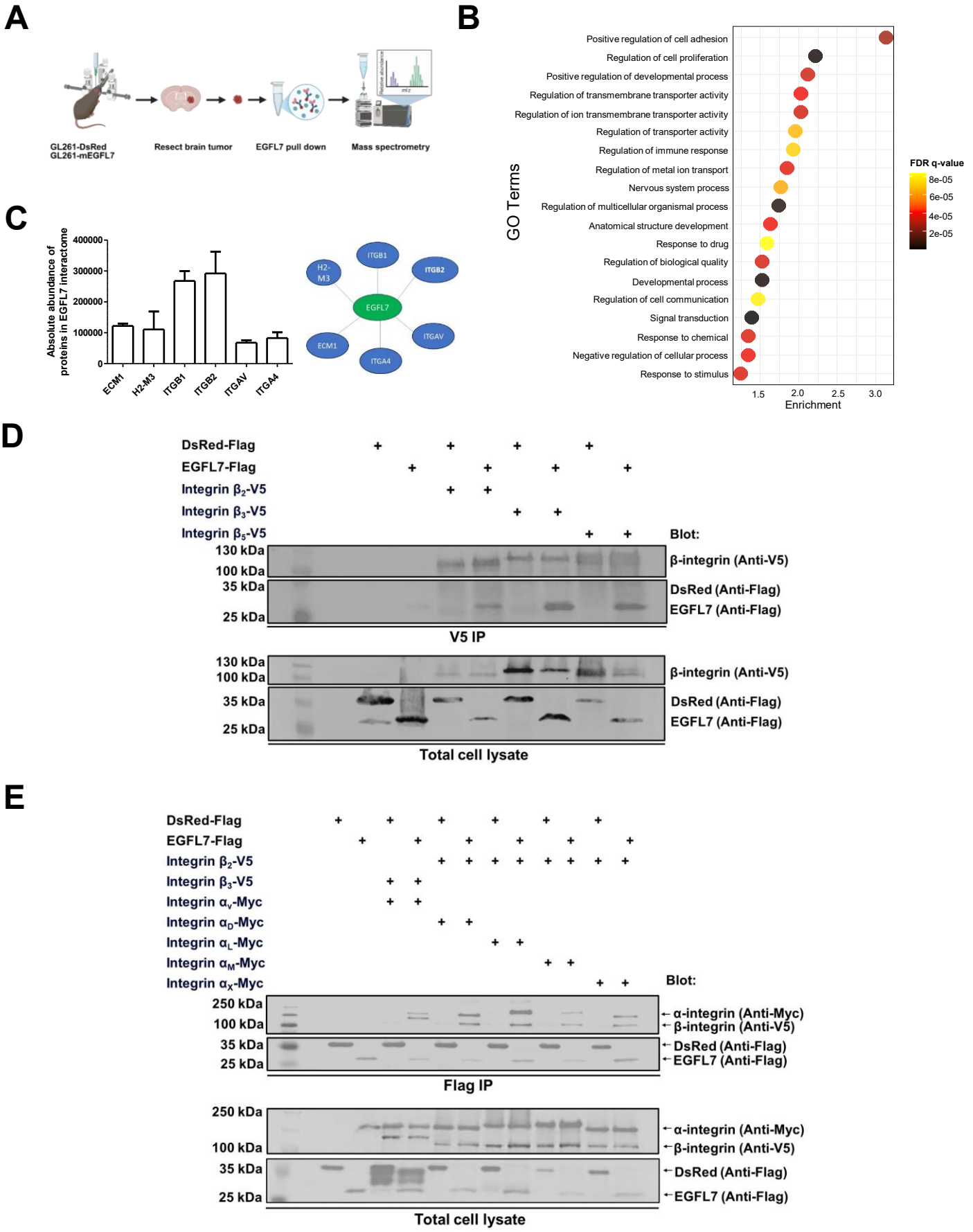
A
GL261-DsRed
GL261-mEGFL7
Resect brain tumor
EGFL7 pull down
Mass spectrometry
B
GO Terms
Positive regulation of cell adhesion
Regulation of cell proliferation
Positive regulation of developmental process
Regulation of transmembrane transporter activity
Regulation of ion transmembrane transporter activity
Regulation of transporter activity
Regulation of immune response
Regulation of metal ion transport
Nervous system process
Regulation of multicellular organismal process
Anatomical structure development
Response to drug
Regulation of biological quality
Developmental process
Regulation of cell communication
Signal transduction
Response to chemical
Negative regulation of cellular process
Response to stimulus
1.5
2.0
2.5
3.0
Enrichment
FDR q-value
8e-05
6e-05
4e-05
2e-05
C
Absolute abundance of proteins in EGFL7 interactome
400000
300000
200000
100000
0
ECM1
H2-M3
ITGB1
ITGB2
ITGAV
ITGA4
EGFL7
D
DsRed-Flag
EGFL7-Flag
Integrin β2-V5
Integrin β3-V5
Integrin β5-V5
Blot:
130 kDa
100 kDa
35 kDa
25 kDa
β-integrin (Anti-V5)
DsRed (Anti-Flag)
EGFL7 (Anti-Flag)
V5 IP
Total cell lysate
E
DsRed-Flag
EGFL7-Flag
Integrin β2-V5
Integrin β3-V5
Integrin αv-Myc
Integrin αD-Myc
Integrin αL-Myc
Integrin αM-Myc
Integrin αX-Myc
Blot:
250 kDa
100 kDa
35 kDa
25 kDa
α-integrin (Anti-Myc)
β-integrin (Anti-V5)
DsRed (Anti-Flag)
EGFL7 (Anti-Flag)
Flag IP
Total cell lysate

Figure 5

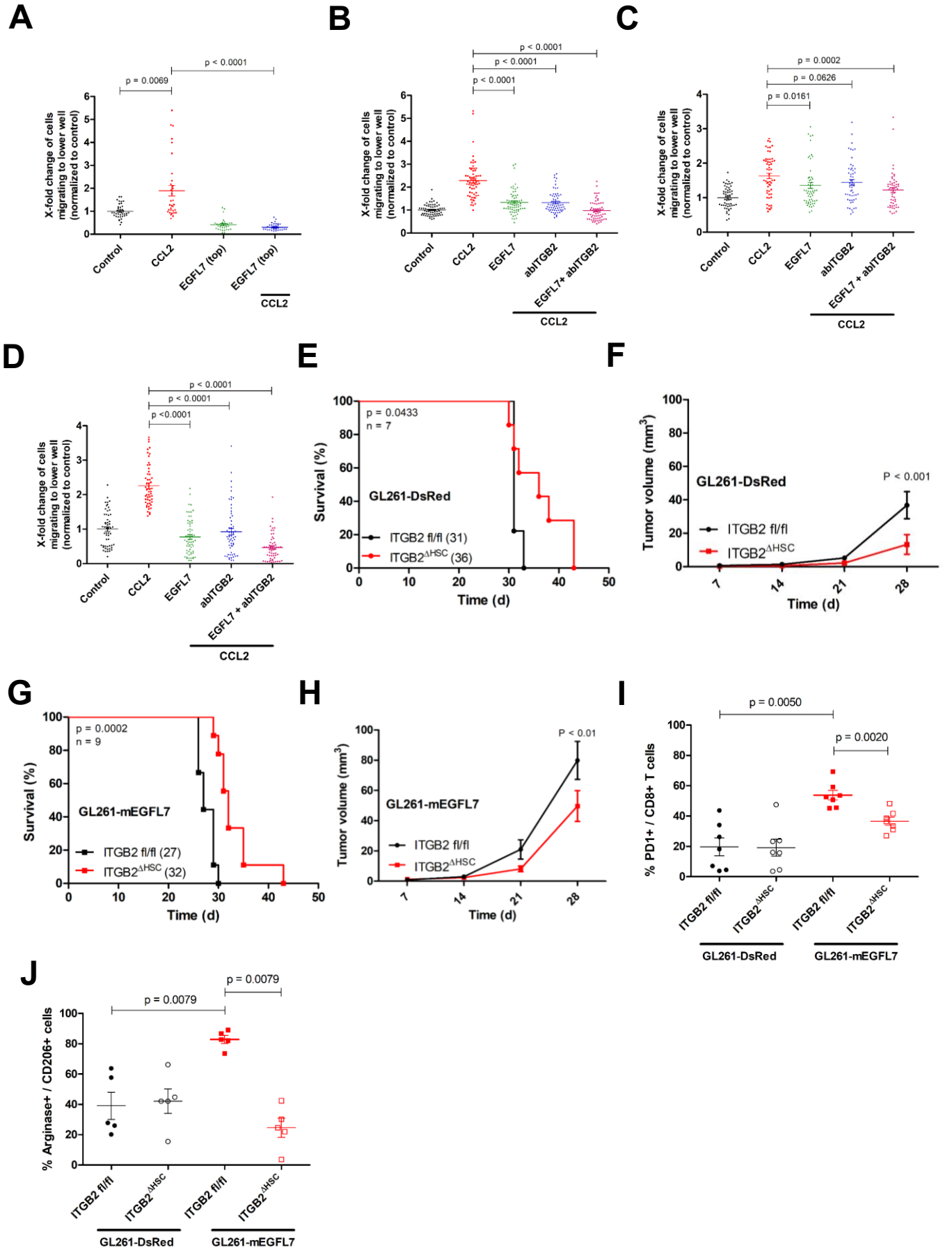
A
p = 0.0069
p < 0.0001
X-fold change of cells migrating to lower well (normalized to control)
Control
CCL2
EGFL7 (top)
EGFL7 (top)
CCL2
B
p < 0.0001
p < 0.0001
p < 0.0001
X-fold change of cells migrating to lower well (normalized to control)
Control
CCL2
EGFL7
abITGB2
EGFL7+ abITGB2
CCL2
C
p = 0.0002
p = 0.0626
p = 0.0161
X-fold change of cells migrating to lower well (normalized to control)
Control
CCL2
EGFL7
abITGB2
EGFL7 + abITGB2
CCL2
D
p < 0.0001
p < 0.0001
p <0.0001
X-fold change of cells migrating to lower well (normalized to control)
Control
CCL2
EGFL7
abITGB2
EGFL7 + abITGB2
CCL2
E
p = 0.0433
n = 7
GL261-DsRed
ITGB2 fl/fl (31)
ITGB2ΔHSC (36)
Survival (%)
Time (d)
F
GL261-DsRed
P < 0.001
ITGB2 fl/fl
ITGB2ΔHSC
Tumor volume (mm3)
Time (d)
G
p = 0.0002
n = 9
GL261-mEGFL7
ITGB2 fl/fl (27)
ITGB2ΔHSC (32)
Survival (%)
Time (d)
H
P < 0.01
GL261-mEGFL7
ITGB2 fl/fl
ITGB2ΔHSC
Tumor volume (mm3)
Time (d)
I
p = 0.0050
p = 0.0020
% PD1+ / CD8+ T cells
ITGB2 fl/fl
ITGB2ΔHSC
ITGB2 fl/fl
ITGB2ΔHSC
GL261-DsRed
GL261-mEGFL7
J
p = 0.0079
p = 0.0079
% Arginase+ / CD206+ cells
ITGB2 fl/fl
ITGB2ΔHSC
ITGB2 fl/fl
ITGB2ΔHSC
GL261-DsRed
GL261-mEGFL7

Figure 6

A

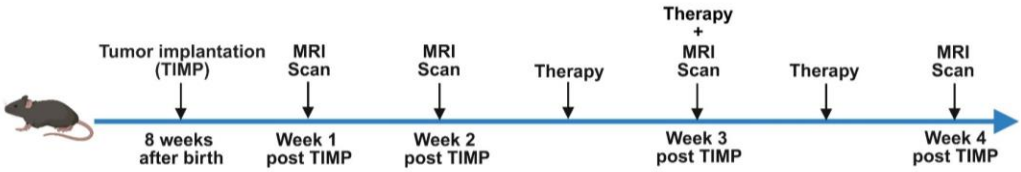
Tumor implantation (TIMP)
MRI Scan
MRI Scan
Therapy
Therapy + MRI Scan
Therapy
MRI Scan
8 weeks after birth
Week 1 post TIMP
Week 2 post TIMP
Week 3 post TIMP
Week 4 post TIMP

B

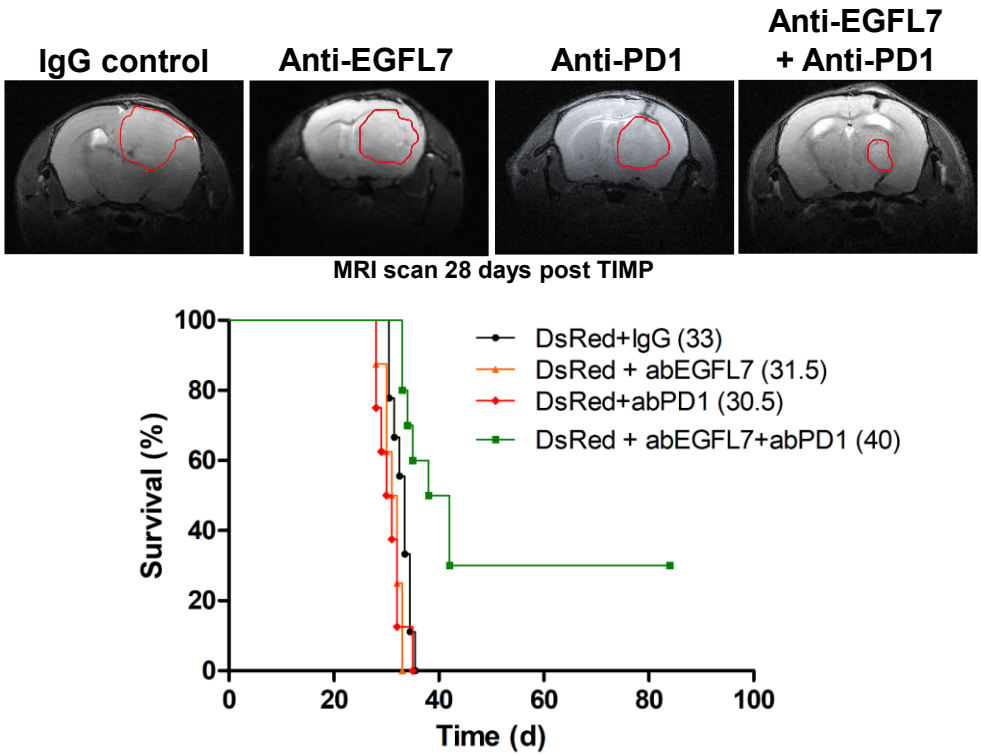
IgG control
Anti-EGFL7
Anti-PD1
Anti-EGFL7 + Anti-PD1
MRI scan 28 days post TIMP
Survival (%)
Time (d)
DsRed+IgG (33)
DsRed + abEGFL7 (31.5)
DsRed+abPD1 (30.5)
DsRed + abEGFL7+abPD1 (40)

C

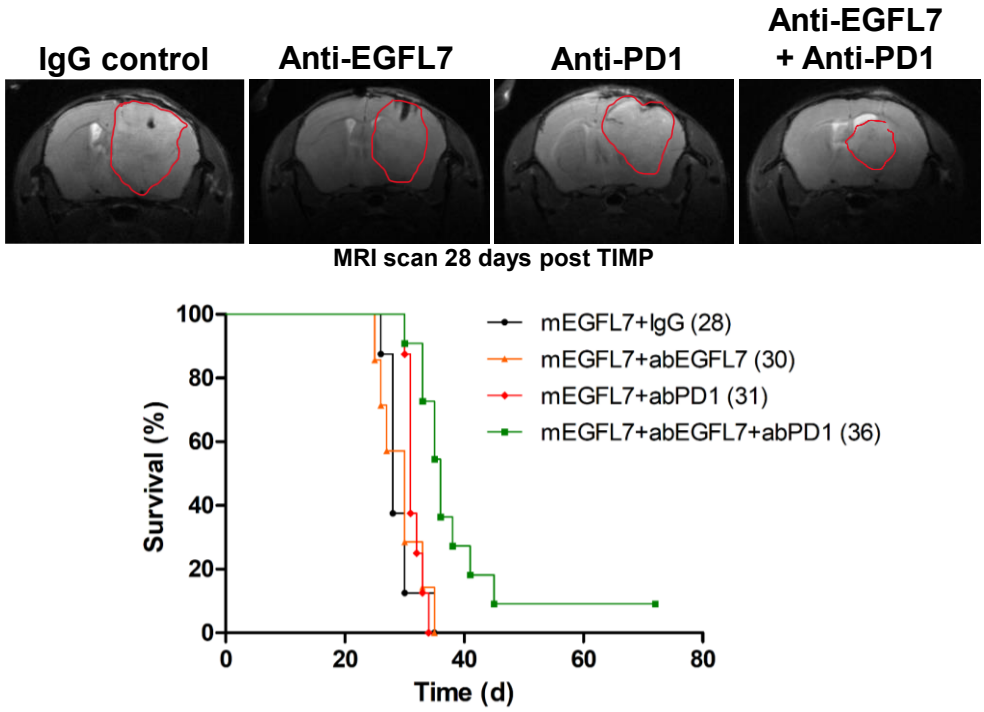
IgG control
Anti-EGFL7
Anti-PD1
Anti-EGFL7 + Anti-PD1
MRI scan 28 days post TIMP
Survival (%)
Time (d)
mEGFL7+IgG (28)
mEGFL7+abEGFL7 (30)
mEGFL7+abPD1 (31)
mEGFL7+abEGFL7+abPD1 (36)

Figure 7

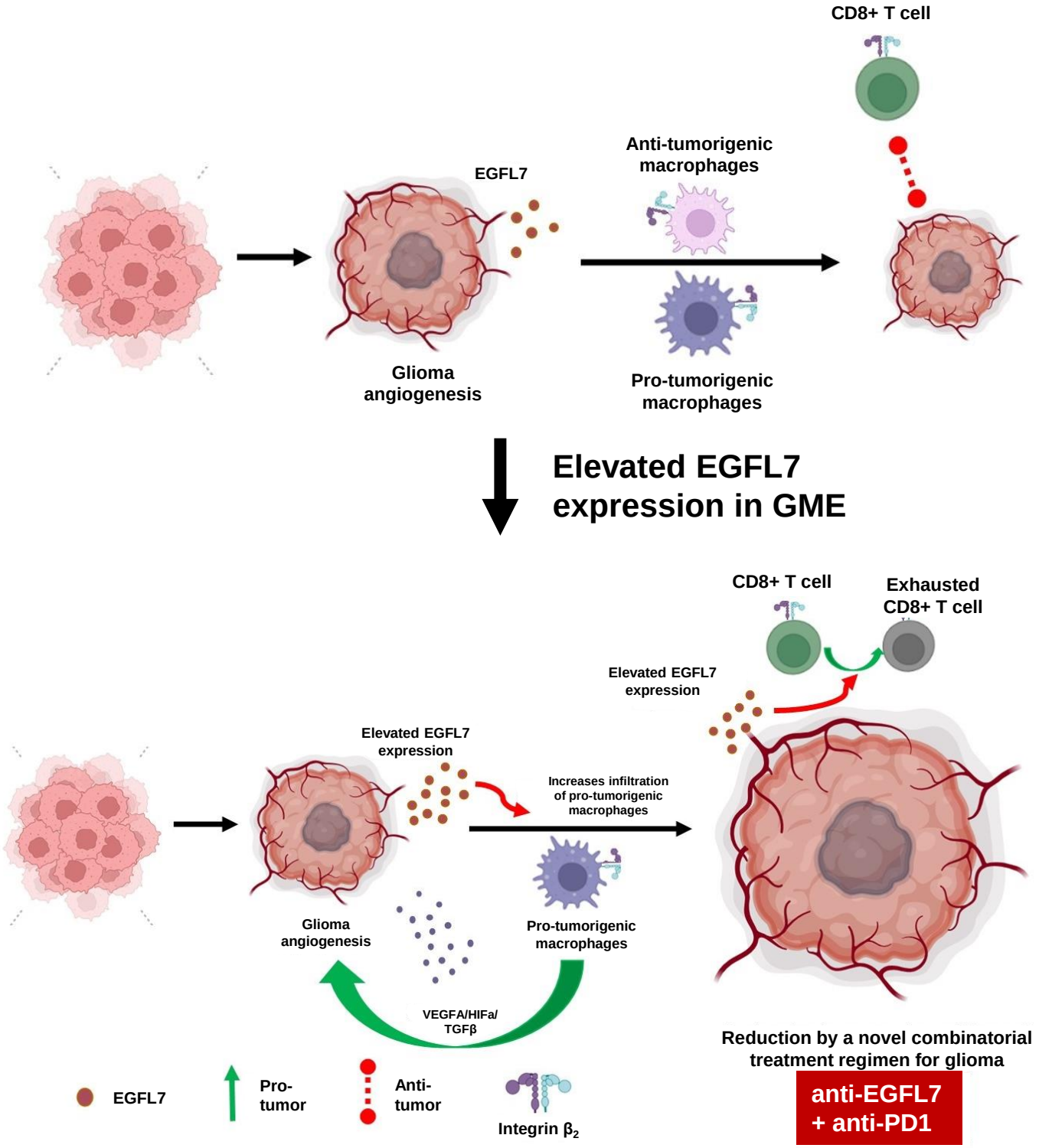
CD8+ T cell
Anti-tumorigenic macrophages
EGFL7
Glioma angiogenesis
Pro-tumorigenic macrophages
Elevated EGFL7 expression in GME
CD8+ T cell
Exhausted CD8+ T cell
Elevated EGFL7 expression
Elevated EGFL7 expression
Increases infiltration of pro-tumorigenic macrophages
Glioma angiogenesis
Pro-tumorigenic macrophages
VEGFA/HIFa/ TGFβ
Reduction by a novel combinatorial treatment regimen for glioma
anti-EGFL7 + anti-PD1
EGFL7
Pro-tumor
Anti-tumor
Integrin β2

Extended Data Fig. 1

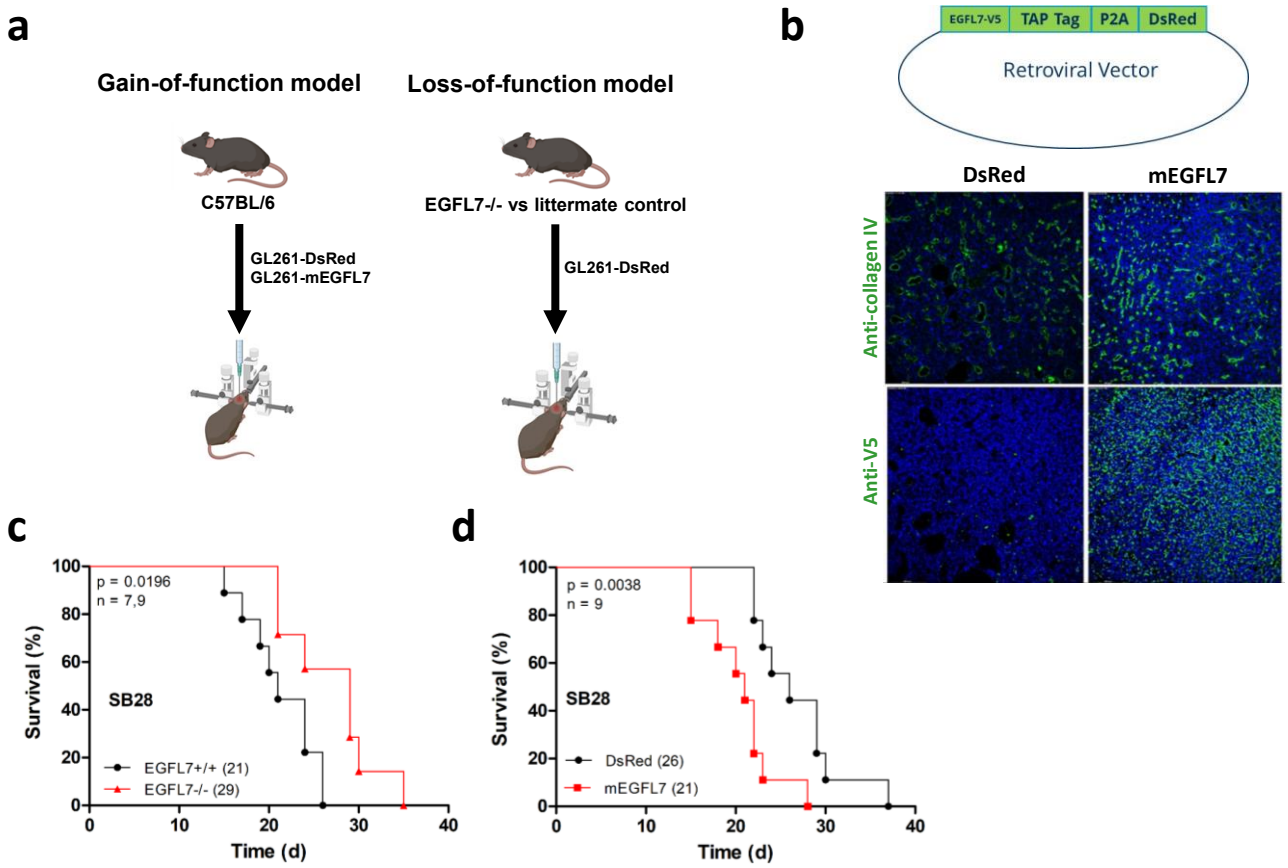

Extended Data Fig. 2

a

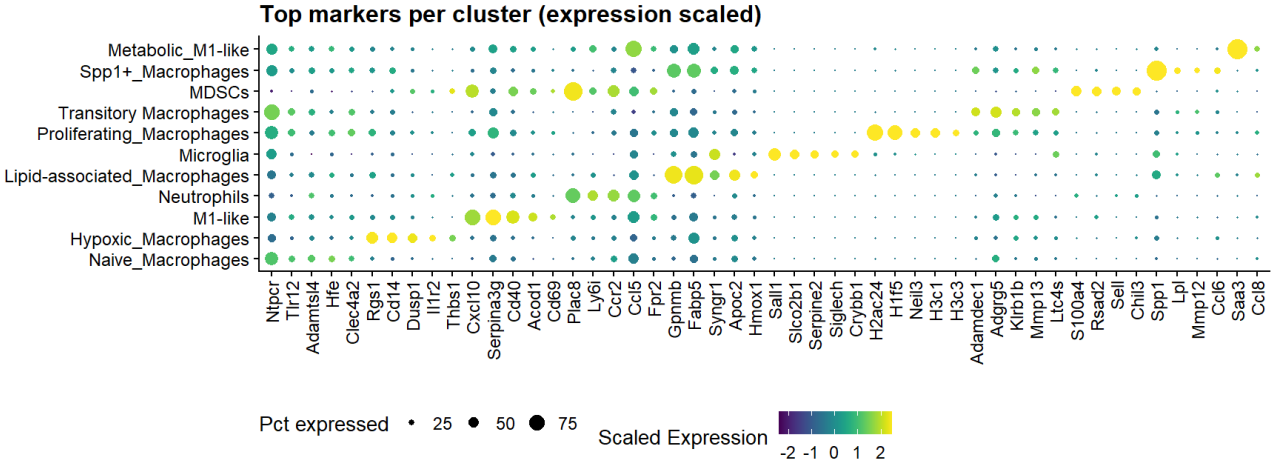

b

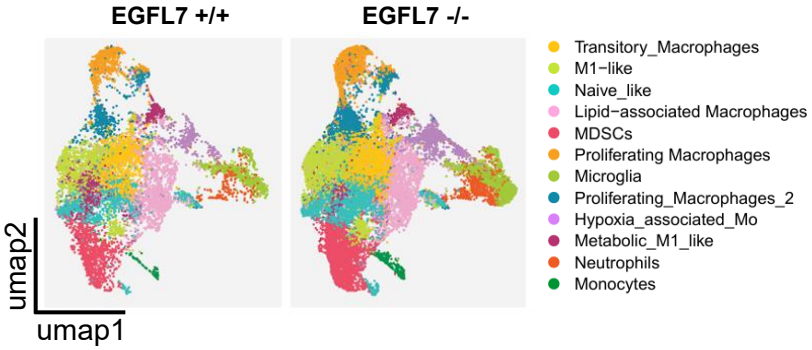

c

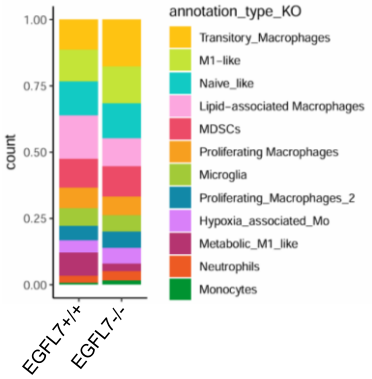

d

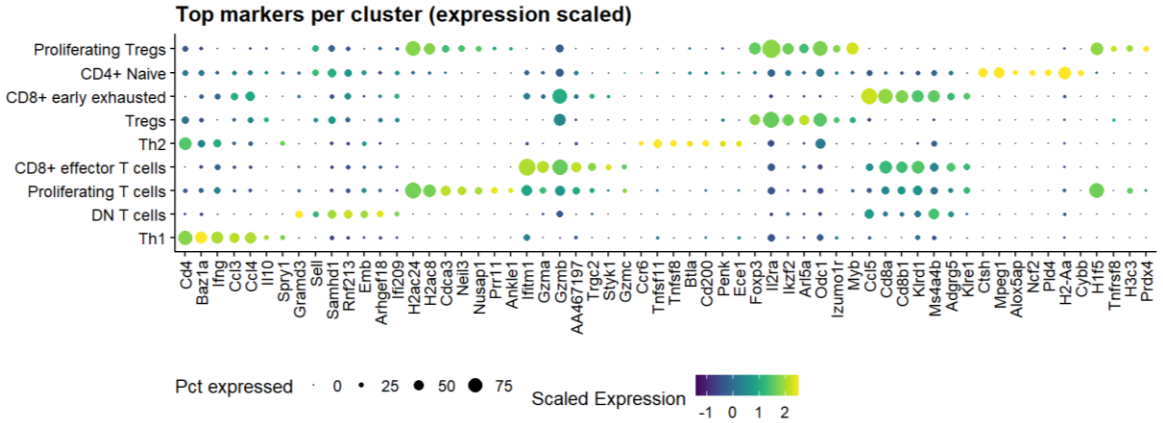

e

f

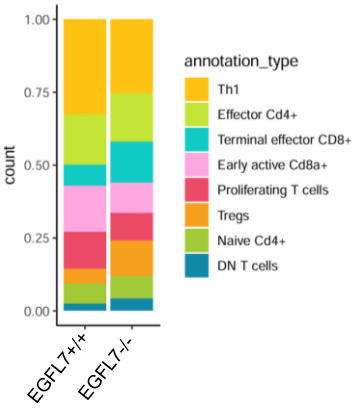

Extended Data Fig. 3

a

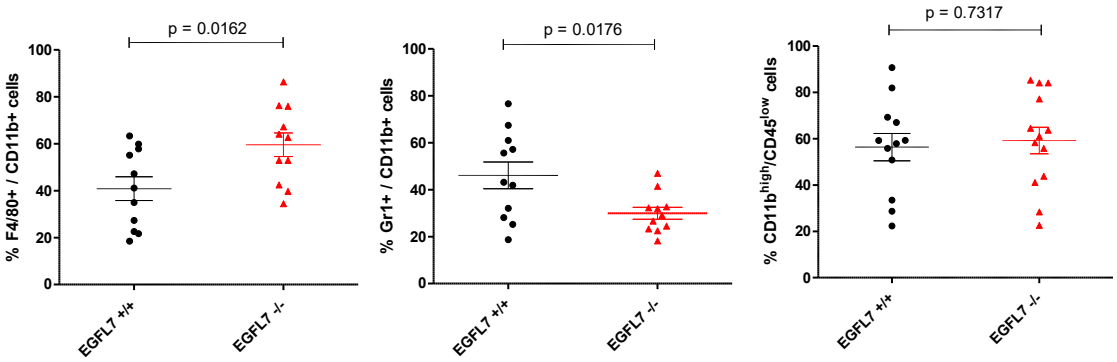

b

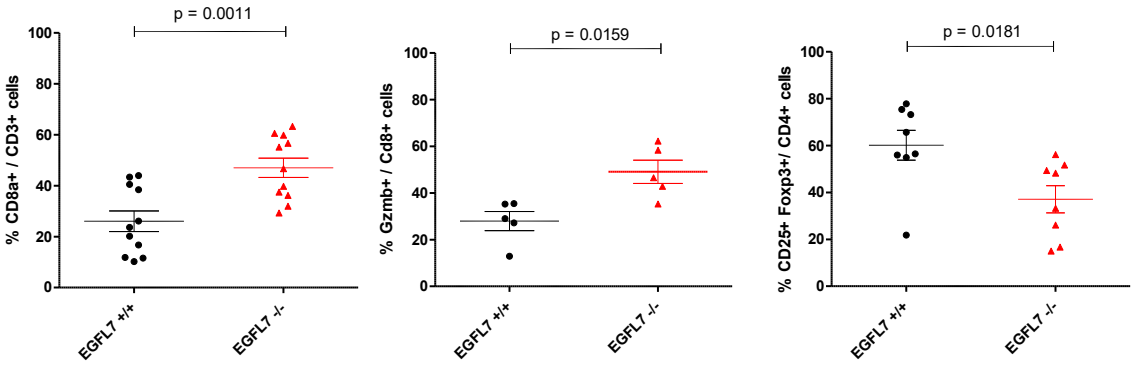
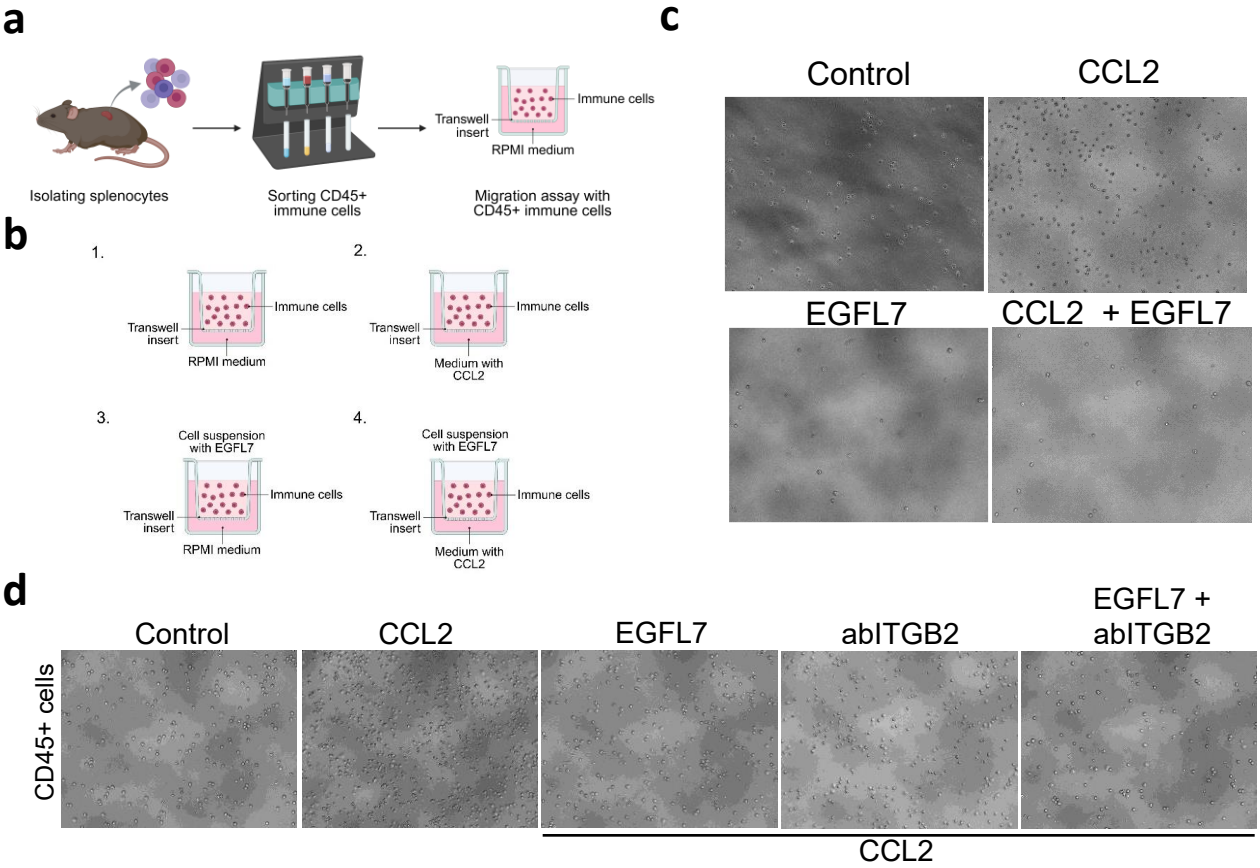
Extended Data Fig. 4